CellPress
OPEN ACCESS

Current Biology

Article

Neural mechanisms underlying uninstructed orofacial movements during reward-based learning behaviors

Wan-Ru Li,[1,2,3,12] Takashi Nakano,[4,5,6,12] Kohta Mizutani,[2,7] Takanori Matsubara,[1,2] Masahiro Kawatani,[1,2,3] Yasutaka Mukai,[2] Teruko Danjo,[1] Hikaru Ito,[8,9] Hidenori Aizawa,[8] Akihiro Yamanaka,[2] Carl C.H. Petersen,[10] Junichiro Yoshimoto,[5,6,11,*] and Takayuki Yamashita[1,2,6,13,14,*]

[1]Department of Physiology, Fujita Health University School of Medicine, 1-98 Dengakugakubo, Kutsukake-cho, Toyoake 470-1192, Japan
[2]Department of Neuroscience II, Research Institute of Environmental Medicine, Nagoya University, Furo-cho, Chikusa-ku, Nagoya 464-8601, Japan
[3]Department of Functional Anatomy & Neuroscience, Graduate School of Medicine, Nagoya University, 65 Tsurumai-cho, Showa-ku, Nagoya 466-8550, Japan
[4]Department of Computational Biology, Fujita Health University School of Medicine, 1-98 Dengakugakubo, Kutsukake-cho, Toyoake 470-1192, Japan
[5]Nara Institute of Science and Technology, 8916-5 Takayama, Ikoma 630-0192, Japan
[6]International Center for Brain Science (ICBS), Fujita Health University, 1-98 Dengakugakubo, Kutsukake-cho, Toyoake 470-1192, Japan
[7]Laboratory for Advanced Brain Functions, Institute for Protein Research, Osaka University, 3-2 Yamadaoka, Suita 565-0871, Japan
[8]Department of Neurobiology, Graduate School of Biomedical and Health Sciences, Hiroshima University, 1-2-3 Kasumi, Minami-ku, Hiroshima 734-8553, Japan
[9]Research Facility Center for Science and Technology, Kagawa University, 1750-1 Ikenobe, Miki-cho, Kita-gun, Kagawa 761-0793, Japan
[10]Laboratory of Sensory Processing, Brain Mind Institute, Faculty of Life Sciences, École Polytechnique Fédérale de Lausanne (EPFL), 1015 Lausanne, Switzerland
[11]Department of Biomedical Data Science, Fujita Health University School of Medicine, 1-98 Dengakugakubo, Kutsukake-cho, Toyoake 470-1192, Japan
[12]These authors contributed equally
[13]Twitter: @tylab_official
[14]Lead contact
*Correspondence: junichiro.yoshimoto@fujita-hu.ac.jp (J.Y.), takayuki.yamashita@fujita-hu.ac.jp (T.Y.)
https://doi.org/10.1016/j.cub.2023.07.013

SUMMARY

During reward-based learning tasks, animals make orofacial movements that globally influence brain activity at the timings of reward expectation and acquisition. These orofacial movements are not explicitly instructed and typically appear along with goal-directed behaviors. Here, we show that reinforcing optogenetic stimulation of dopamine neurons in the ventral tegmental area (oDAS) in mice is sufficient to induce orofacial movements in the whiskers and nose without accompanying goal-directed behaviors. Pavlovian conditioning with a sensory cue and oDAS elicited cue-locked and oDAS-aligned orofacial movements, which were distinguishable by a machine-learning model. Inhibition or knockout of dopamine D1 receptors in the nucleus accumbens inhibited oDAS-induced motion but spared cue-locked motion, suggesting differential regulation of these two types of orofacial motions. In contrast, inactivation of the whisker primary motor cortex (wM1) abolished both types of orofacial movements. We found specific neuronal populations in wM1 representing either oDAS-aligned or cue-locked whisker movements. Notably, optogenetic stimulation of wM1 neurons successfully replicated these two types of movements. Our results thus suggest that accumbal D1-receptor-dependent and -independent neuronal signals converge in the wM1 for facilitating distinct uninstructed orofacial movements during a reward-based learning task.

INTRODUCTION

It has long been known that the movements of animals, such as locomotion and whisking, profoundly influence neuronal activity within sensory cortices.[1–3] Recent large-scale neural recordings have suggested that this motor-related neuronal modulation is not confined to a specific area but is pervasive throughout cortical and subcortical brain regions.[4–9] Furthermore, in animals engaged in cognitive tasks, movements that are neither instructed nor necessary for task execution can be aligned to task events and significantly contribute to task-aligned neuronal activity.[5–8] In particular, orofacial movements, i.e., movements of facial parts surrounding the mouth, such as the nose and whiskers, strongly correlate with brain-wide neuronal activities in mice.[4,5,9] However, the mechanisms by which the brain generates and coordinates orofacial movements, uninstructed but task-aligned, remain largely elusive.

Mice well-trained for a stimulus-reward association task frequently exhibit whisker movements (WMs) immediately following a reward-predicting cue presentation.[5,10–13] The

CellPress
OPEN ACCESS

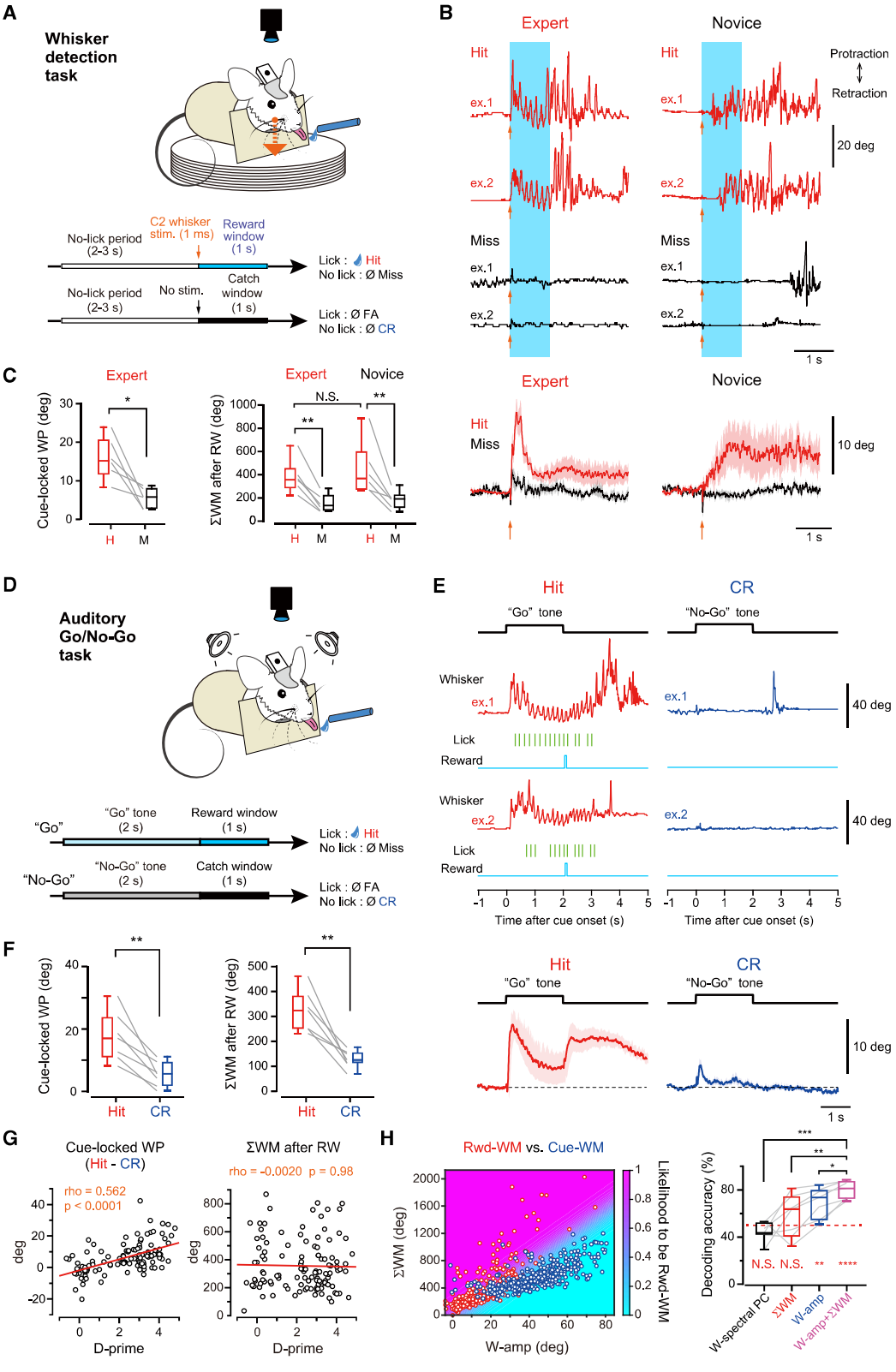

(legend on next page)

acquisition of liquid rewards through licking also seems to elicit whisker and other facial movements.[5,10–13] These orofacial movements are often regarded as part of facial expressions related to reward expectation and acquisition.[12,14,15] However, given that licking behavior is phase-locked to breathing, sniffing, and other orofacial activities,[16–18] it remains equivocal whether such orofacial movements are simply concurrent with goal-directed actions or are instead driven by independent neural mechanisms. Moreover, nothing is currently known about which neuronal populations are directly involved in forming task-aligned, uninstructed orofacial movements.

Dopamine (DA) neurons in the ventral tegmental area (VTA) play a central role in mediating motivated behaviors and are supposed to form part of the reward circuit of the brain.[19–21] Transient stimulation of VTA-DA neurons is reinforcing[22–24] and can replace some aspects of liquid reward.[25] The VTA-DA neurons in mice fire phasically upon reward expectation and acquisition,[26–28] the timings similar to uninstructed WMs in reward-based tasks.[5,10,11] Therefore, the VTA-DA neurons may be involved in making uninstructed orofacial movements.

The primary motor cortex (M1) is another candidate for a brain region that may be involved in uninstructed orofacial movements. There has been compelling evidence that stimulation of the orofacial M1 of rodents triggers movements in the whisker and nose.[29–33] Neurons in the orofacial M1 encode various aspects of movements in the whisker and nose.[34–36] Nevertheless, it is unknown whether the orofacial M1 plays a causal role in constituting uninstructed orofacial movements during reward-based tasks.

In this study, we show that distinct WMs are induced upon reward-predicting cue presentation and reward-acquiring reaction. Using optogenetic stimulation of VTA-DA neurons (oDAS), we demonstrate that these two types of orofacial movements could also be elicited without goal-directed action. Our perturbational analyses revealed that the mesolimbic DA pathway is essential in driving oDAS-aligned orofacial movements but not cue-locked ones, while whisker M1 (wM1) is a critical circuit node for driving these two types of movements. Based on these findings, we propose a neural circuit model where neuronal signals converge into wM1 for facilitating uninstructed orofacial movements during a reward-based learning task.

RESULTS

Whisker movements during reward-based learning tasks

To examine task-aligned, uninstructed orofacial movements of mice, we first analyzed the WM data in our previous recordings.[37] These recordings involved mice performing a whisker detection task, in which thirsty mice were trained to lick for a water reward in response to a whisker deflection[10,37] (Figure 1A). Expert mice well-trained for the task exhibited a rapid whisker protraction (WP) immediately after the reward-associated, brief (1 ms) whisker stimulation in hit trials (Figure 1B), which had a significantly larger amplitude compared with miss trials (hit 15.8° ± 2.2°, miss 5.6° ± 1.0°, n = 6 mice, p = 0.013; Figure 1C). Such a rapid cue-locked WP in hit trials was absent in novice mice with low task proficiency (Figure 1B), suggesting that the cue-locked WP becomes evident after learning the task. These expert mice also showed active WMs after reward acquisition in hit trials, some of which appeared similar to exploratory whisking[30–32] (Figure 1B). Total WMs (ΣWM) during 1 s after the reward time window were larger in hit trials than in miss trials (hit 381° ± 59°, miss 156° ± 31°, n = 6 mice, p = 0.0052, Bonferroni's multiple comparison test; Figure 1C). In contrast to the learning-dependent nature of the cue-locked WMs, task learning did not change the ΣWM after hits (novice hit 444° ± 96°, n = 6 mice, p = 0.93, Bonferroni's multiple comparison test vs. expert hit; Figure 1C).

We next examined whether the task-aligned WMs seen in the whisker detection task are specific for a task involving whisker sensation. We trained mice for an auditory Go/No-Go task where whisker sensation or motion is not required for task execution. We set the reward time window (1 s) after a 2-s auditory cue presentation (Figure 1D) to well separate the timings of expectation and acquisition of water reward. Expert mice for the auditory task exhibited a rapid cue-locked WP (17.4° ± 3.0°, n = 7 mice) and active WMs after reward acquisition (ΣWM 0–1 s after the reward window, 320° ± 32°, n = 7 mice) in hit trials, both of which were

Figure 1. Stereotypical whisker movements during stimulus-reward association tasks

(A) Schematic for the whisker detection task. FA, false alarm; CR, correct rejection.

(B) Top, example traces of the whisker position in hit (red) and miss (black) trials during the whisker detection task, obtained from an expert (left) and novice (right) mouse. Arrow, whisker stimulation. Light blue shadow, the reward time window (RW). Bottom, grand average traces of the whisker position (n = 6 mice for each). Shadows indicate ±SEM.

(C) Amplitudes of the cue-locked WP (left) and the ΣWM 0–1 s after RW (right), in hit (H) and miss (M) trials during the whisker detection task (n = 6 mice for each). ** p < 0.01, *p < 0.05; N.S., not significant; paired t test (cue-locked WP) and Bonferroni's multiple comparison test (ΣWM after RA).

(D) Schematic for the auditory Go/No-Go task.

(E) Example (top) and grand average (bottom, n = 7 expert mice for each) traces of the whisker position in hit (red) and CR (blue) trials, and other task variables during the auditory Go/No-Go task.

(F) Cue-locked WP amplitude (left) and ΣWM 0–1 s after RW (right) during the auditory Go/No-Go task (n = 7 expert mice). **p < 0.01, paired t test.

(G) Left, the difference in the cue-locked WP amplitude between hit and CR trials (left) and ΣWM 0–1 s after RW of hit trials (right) as a function of task proficiency (d-prime), obtained from 10 mice. Red, linear regression line.

(H) Left, an example decoding analysis of WMs at 0–1 s after the cue onset (Cue-WM, blue) and 0–1 s after RW (Rwd-WM, red), obtained from an expert mouse. Right, decoding accuracies by the models for discrimination between Cue-WM and Rwd-WM (see STAR Methods) (n = 7 for each). The dashed red line indicates the chance level. ****p < 0.0001, ***p < 0.001, ** p < 0.01, *p < 0.05; N.S., not significant; Dunnett's multiple comparison test vs. W-amp + ΣWM (shown in black) or one-sample t test vs. chance level (shown in red).

Thin lines in (C), (F), and (H) and open circles in (G) and (H) indicate individual data.

See also Figure S1.

CellPress
OPEN ACCESS

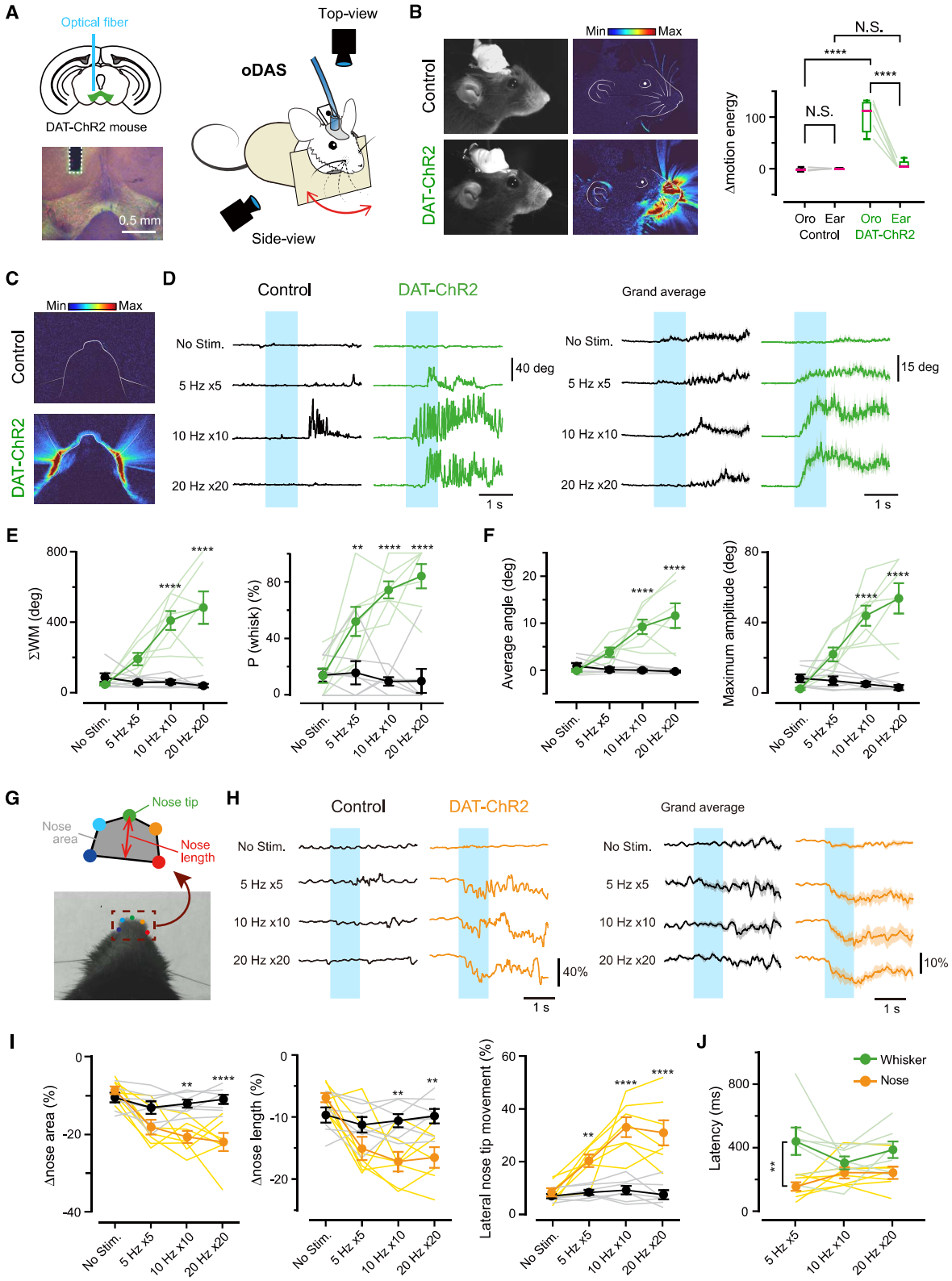

Figure 2. Orofacial movements induced by transient activation of VTA-DA neurons

(A) Left, schematic for the optical fiber location for the oDAS experiments (top), and an epifluorescence image of a coronal section containing VTA and the trace of the inserted fiber (dashed line) (bottom). Green, ChR2-eYFP; red, tyrosine hydroxylase; blue, DAPI. Right, schematic for the oDAS experiment.

(legend continued on next page)

more prominent than in correct rejection (CR) trials (Figures 1E and 1F). In the auditory task, both Go and No-Go sound cues equally elicited a rapid WP in novice mice (Figures S1A and S1B), which might be a reflex motor action to a salient auditory stimulus. However, the difference in the amplitude of the cue-locked WP between hits and CR trials became more prominent as the mice learned the task (Figure 1G). In contrast, task learning did not change ΣWM after hits (Figure 1G). These results are essentially the same as those in the whisker detection task. Our machine-learning models accurately discriminated between WMs during hit trials and those during CR trials in expert mice (Figure S1C), indicating that the movements of a single whisker can provide information about the behavioral states of mice. Additionally, our models could distinguish between cue-locked WMs and those that occurred after reward acquisition, with a decoding accuracy of 79.9 ± 2.9% (by a model that uses ΣWM and WP amplitude, n = 7 mice, $p < 0.0001$, one-sample t test against the chance level [50%]; Figure 1H). Thus, WMs with distinct properties are observed at the timings of reward expectation and a second after reward acquisition in stimulus-reward association tasks.

Orofacial movements evoked by oDAS

The uninstructed WMs seen in our reward-based tasks (Figure 1) may be associated with anticipatory or reward-acquiring licking, which has a specific pattern frequency (5–8 Hz) and is phase-locked to WMs[16–18] (Figures S1D–S1F). We next built an experimental setting to reward mice without inducing any motor actions required for task execution. We implanted an optic fiber unilaterally over the VTA of transgenic mice expressing channelrhodopsin 2 (ChR2) in DA neurons (DAT-ChR2, Figure 2A). We first tested whether a brief (1 s) train of optogenetic stimulation of the VTA-DA neurons (named oDAS), which is known to be rewarding and reinforcing,[22–25] can induce facial movements. An oDAS with 20 pulses at 20 Hz elicited facial movements at the rostral parts, including whiskers and nose, but not around ears and eyes, in awake head-restrained mice (Figure 2B). We therefore further analyzed oDAS-induced whisker and nose movements by monitoring the frontal face of mice from a top view (Figures 2C–2J; Video S1). Our strongest oDAS with 20 pulses at 20 Hz induced rhythmic whisking with a high probability (83.8 ± 8.5%, n = 7 mice; Figure 2F). The average whisker angle during oDAS was protracted by 11.6° ± 2.6° (n = 7 mice, 20 pulses at 20 Hz; Figure 2F). The probability of whisking initiation, ΣWM during oDAS, and the average and maximum amplitude of WMs all increased, depending on the stimulus frequency (Figures 2D–2F) and photo-stimulus intensity (Figures S2A and S2B). In contrast, in control Ai32 mice without ChR2-expression, photostimulation of VTA did not evoke any consistent WMs (Figures 2D–2F, S2A, and S2B). Such protracted rhythmic whisking evoked by oDAS resembled WMs upon reward acquisition in reward-based learning tasks (Figures 1B and 1F). The oDAS-induced whisking had an average latency of 402 ± 51 ms (n = 7 mice, with 20 pulses at 20 Hz; Figure 2J).

We next analyzed nose movements evoked by oDAS using a deep learning-based toolbox DeepLabCut[38] (Figure 2G). Mice exhibited nose twitches upon oDAS: the top-view nose area decreased (peak change from baseline [Δnose area]: 22.0 ± 2.3%, n = 7) (Figures 2H and 2I), and the nose length in an anterior-posterior axis became shortened (peak change from baseline [Δnose length]: 16.5 ± 1.6%, n = 7) (Figure 2I), indicating contractions of the nasal muscle. The oDAS also induced a lateral movement of the nose tip (peak lateral movement as the percentage of the mean baseline nose length [lateral nose tip movement]: 31.0 ± 4.8%, n = 7) (Figure 2I). The magnitude of such nose movements depended on the stimulus frequency (Figures 2H and 2I) and photo-stimulus intensity (Figures S2A and S2C) and was highly correlated with WMs (Figure S2D). The latencies of nose movement initiation and whisking initiation were similar, except for when using the weakest stimulation (Figure 2J). Thus, transient activation of VTA-DA neurons is sufficient to facilitate movements in the whisker and nose. In contrast, optogenetic stimulation of DA neurons in the substantia nigra pars compacta (SNc), which are implicated in the coordination of locomotion in mice,[39,40] did not induce whisker and nose movements (Figures S2E–S2G).

Orofacial movements time-locked to reward-predicting cues

We next examined whether the cue-locked WP can be induced without anticipatory or goal-directed licking. We presented a sound cue (5 s) paired with oDAS during the last 1 s of the cue to head-restrained DAT-ChR2 or control (Ai32) mice (Figures 3A and 3B). Mice experienced ~20 trials of the paired stimulation per day, with random intertrial intervals between 180 and 240 s. On the first day of this conditioning (day 1), both DAT-ChR2 and control mice similarly exhibited a WP immediately after the sound presentation with a high probability (Figure 3C), which might represent a reflex motor action to a salient auditory stimulus as observed in the auditory Go/No-Go task

(B) Left, single example video frames from individual mice. Middle, motion energy heatmaps overlaid onto the face line drawings from the mice shown in left. Right, quantifications for motion energy around the orofacial part (Oro) and the ear during oDAS. Medians of the boxplots are shown in red.
(C) Example motion energy heatmaps overlaid onto the top-view face line.
(D) Left, example traces of the whisker position upon oDAS (light blue shadow) with different stimulus frequencies, obtained from a control (black) and DAT-ChR2 (green) mouse. Right, grand average of the whisker position upon oDAS (control: n = 7 mice; DAT-ChR2: n = 7 mice). Shadows of traces: ±SEM.
(E) ΣWM (left) and P (whisk) (the probability of whisking initiation, right) during oDAS.
(F) Average (left) and maximal (right) amplitude of whisker angle during oDAS.
(G) Schematic for the nose analysis (top) and a top-view snapshot of mouse face (bottom).
(H) Same as (B) but for traces of the top-view nose area from control (black) or DAT-ChR2 (orange) mice.
(I) Quantifications for the changes in nose area (left), nose length in the anterior-posterior axis (middle), and lateral movements of the nose tip (right).
(J) Latencies of movement of the whisker (green) and nose (orange) upon oDAS.
Filled circles and error bars show mean ± SEM. Lightly colored lines correspond to individual data. ****$p < 0.0001$, **$p < 0.01$; N.S., not significant; Bonferroni's multiple comparison test, control vs. DAT-ChR2 in (E), (F), and (I) or whisker vs. nose in (J).
See also Figures S1 and S2 and Video S1.

CellPress
OPEN ACCESS

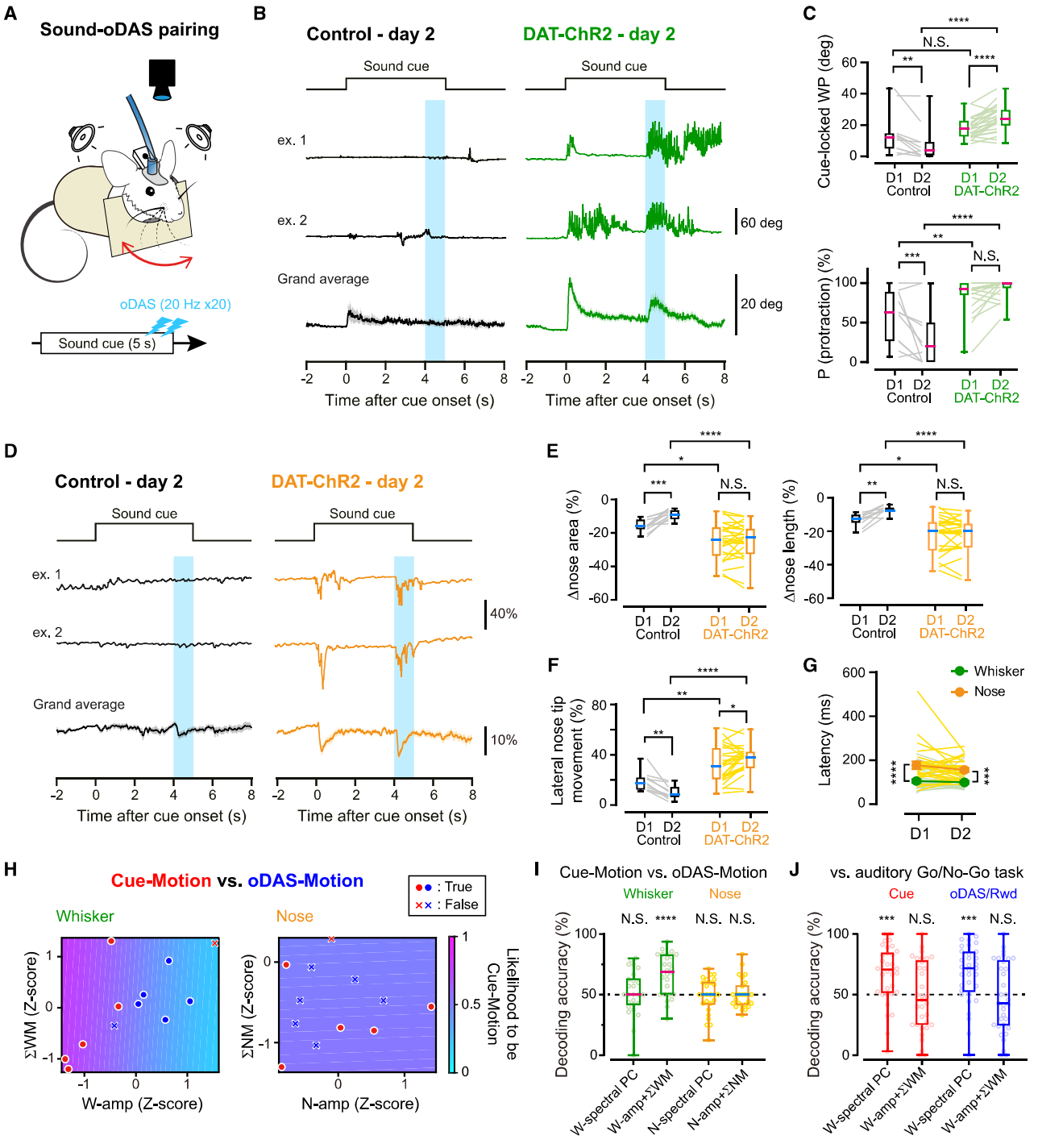

Figure 3. Orofacial movements during a stimulus-oDAS association task

(A) Schematic for the sound-oDAS pairing conditioning.

(B) Example and grand average traces of the whisker position during the sound-oDAS pairing conditioning on day 2, obtained from a control (black) and DAT-ChR2 (green) mouse (control: n = 11 mice; DAT-ChR2: n = 26 mice). The timings of the sound cue presentation (black line) and oDAS (light blue shadow) are indicated. Shadows of grand average traces: ±SEM.

(C) The amplitude of cue-locked WP (top) and P (protraction) (protraction probability, bottom) on days 1 (D1) and 2 (D2).

(D) Same as (B) but for traces of the top-view nose area from control (black) or DAT-ChR2 (orange) mice.

(E) Quantifications for the changes in the nose area and nose length at the cue onset.

(F) Quantifications for the changes in lateral movements of the nose tip at the cue onset.

(G) Latencies of cue-locked WP (green) and nose tip movements (orange) upon sound cue presentation.

(legend continued on next page)

(Figures S1A and S1B). On day 2, however, DAT-ChR2 mice exhibited a rapid, cue-locked WP (24.3° ± 1.6°, n = 26 mice) (Figure 3B) with a significantly larger magnitude than that on day 1 (18.3° ± 1.3°, n = 26 mice, $p < 0.0001$, Bonferroni's multiple comparison test; Figures 3C and S3A). The magnitude of the cue-locked WP continued to increase over 4 days of learning (Figure S3B). In contrast, in control mice, the magnitude and probability of the cue-locked WP significantly decreased on day 2 (Figures 3B, 3C, and S3A). These results indicate that learning the sound-oDAS pairing can elicit cue-locked WP even in the absence of goal-directed action. The latency of WP after the onset of the sound presentation was 98 ± 7 ms (n = 26 mice) on day 2 (Figure 3G), which was significantly shorter than that of oDAS-induced whisker motion ($p < 0.0001$, with 20 pulses at 20 Hz, Mann-Whitney *U* test, Figure 2J). In addition to the WP, a quick nose twitch was also elicited immediately after the sound onset in DAT-ChR2 mice on day 2 (Δnose area: 25.1 ± 2.2%, n = 26 mice; Δnose length: 22.2 ± 2.0%, n = 26 mice; lateral nose tip movement: 36.1 ± 2.2%, n = 26 mice), which was absent in control mice without ChR expression on day 2 (Figures 3D–3F). The latency of the cue-locked nose twitch (156 ± 10 ms, n = 26 mice) was significantly longer than that of the cue-locked WP ($p = 0.0008$, two-way ANOVA; Figure 3G) but still shorter than that of oDAS-induced nose movement (257 ± 38 ms, upon oDAS at 20 Hz for 1 s, n = 7 mice, $p = 0.0006$, unpaired t test). The amplitudes of the nose twitch and WP at the cue onset were weakly but significantly correlated (Figure S3C). Control mice showed small reflex movements in the whisker and nose at the cue onset in a small fraction of the trials on day 1 (Figures 3C, 3E, 3F, and S3A). Its magnitude and probability significantly decreased with training (Figures 3C, 3E, 3F, and S3A), suggesting that learning of sound-oDAS association should cause the cue-locked orofacial motions in DAT-ChR2 mice on day 2. The magnitude of WMs and the probability of whisking during oDAS in this task did not change over 5 days, with a slight tendency to be attenuated after 3 days, although not statistically significant (Figure S3D).

Our machine-learning models, utilizing ΣWM and WP amplitude, could distinguish oDAS-induced and cue-locked WMs (decoding accuracy, 66.6 ± 3.4%, n = 26, $p < 0.0001$, one-sample t test against the chance level [50%]; Figures 3H and 3I). This suggests that the reward-predicting cue and oDAS induce WMs with distinct properties. However, our models based on nose movements were unable to predict the timing of the data (cue onset or during oDAS) (Figures 3H and 3I). Additionally, we compared WMs during the sound-oDAS and auditory Go/No-Go tasks. The models based on ΣWM and WP amplitude could not distinguish cue-locked or oDAS/reward-aligned WMs induced in these two types of tasks (Figure 3J). However, the models based on the spectral principal component (PC) could discriminate between them (Figure 3J). The spectral PC primarily derives from oscillatory WMs associated with goal-directed licking (Figures S1C–S1F). These results suggest that WMs during the sound-oDAS pairing task are indistinguishable from those during water-reward-based learning tasks, except for the presence of licking-associated oscillatory movements.

Involvement of accumbal D1R in driving orofacial movements

We next investigated the neuronal circuits downstream of VTA-DA neurons for inducing orofacial movements. Stimulation of VTA-DA neurons is known to activate medium spiny neurons expressing D1 receptors (D1Rs) in the nucleus accumbens (NAc) through the mesolimbic DA pathway.[41] We therefore examined the role of D1Rs in oDAS-induced orofacial movements. Intraperitoneal (i.p.) injection of a D1R antagonist, SCH23390 (0.3 mg/kg), abolished the oDAS-induced whisking (ΣWM: saline = 487° ± 127° [n = 7 mice], SCH23390 = 32.4° ± 5.3° [n = 7 mice], $p = 0.013$, paired t test; whisking probability: saline = 81.6 ± 11.2% [n = 7 mice], SCH23390 = 5.4 ± 5.4% [n = 7 mice], $p = 0.031$, Wilcoxon signed rank test) and nose twitches (Δnose area: saline = 25.0 ± 5.5% [n = 7 mice], SCH23390 = 5.0 ± 1.3% [n = 7 mice], $p = 0.011$, paired t test) in DAT-ChR2 mice (Figures 4A, 4B, and S4A), suggesting the involvement of D1Rs. The i.p. injection of SCH23390 also reduced the spontaneous WMs (Figure 4A), suggesting a general sedative effect of the drug. To specifically examine the role of D1Rs in the NAc, we used CRISPR-Cas9-mediated *in vivo* genome editing. We knocked out D1Rs in the NAc of DAT-ChR2 mice by local injection of an adeno-associated virus (AAV) vector harboring saCas9 with guide RNA targeting the *Drd1a* gene (AAV-gRNA), which has been previously shown to have a high cleavage rate[42] and no off-target effects (Figures 4C, S4B, and S4C). These NAc-D1R-knockout (KO) mice did not show WMs or nose twitches upon oDAS (Figures 4C, 4D and S4D). In contrast, control mice injected with a control AAV saCas9-gRNA vector (AAV-control) exhibited oDAS-induced orofacial motions (Figures 4C, 4D, and S4D). Spontaneous WMs were unaffected in NAc-D1R-KO mice (Figure 4C). These results suggest the involvement of accumbal D1Rs in oDAS-induced orofacial movements. Moreover, optogenetic activation of the axons of VTA-DA neurons in the NAc induced WMs and nose twitches (Figures 4E, 4F, and S4E). Our results thus indicate that the mesolimbic DA pathway mediates oDAS-induced orofacial movements by activating accumbal D1Rs.

We further tested whether D1Rs are also involved in generating the cue-locked WP. We performed an i.p. injection of saline or SCH23390 in the mice that had learned the sound-oDAS

(H) Example decoding analyses of whisker (left) and nose (right) movements at 0–1 s after the cue onset (red, Cue-Motion) and during 1-s oDAS (blue, oDAS-Motion), obtained from a mouse on day 2 (see STAR Methods). True, correctly predicted; false, incorrectly predicted.
(I) Decoding accuracies by the models for discrimination between cue-locked and oDAS-aligned whisker/nose movements during the sound-oDAS task (n = 26 mice). The dotted line indicates the chance level.
(J) Same as (I) but for discrimination between whisker motions during the sound-oDAS task and those during the auditory Go/No-Go task.
Medians of the boxplots in (C), (E), (F), and (I) are shown in magenta or cyan. Filled circles and error bars in (G) show mean ± SEM. Lightly colored lines correspond to individual data. ****$p < 0.0001$, ***$p < 0.001$, **$p < 0.01$; N.S., not significant; two-way ANOVA followed by Bonferroni's multiple comparison test, except for one-sample t test vs. the chance level in (I).
See also Figure S3.

CellPress
OPEN ACCESS

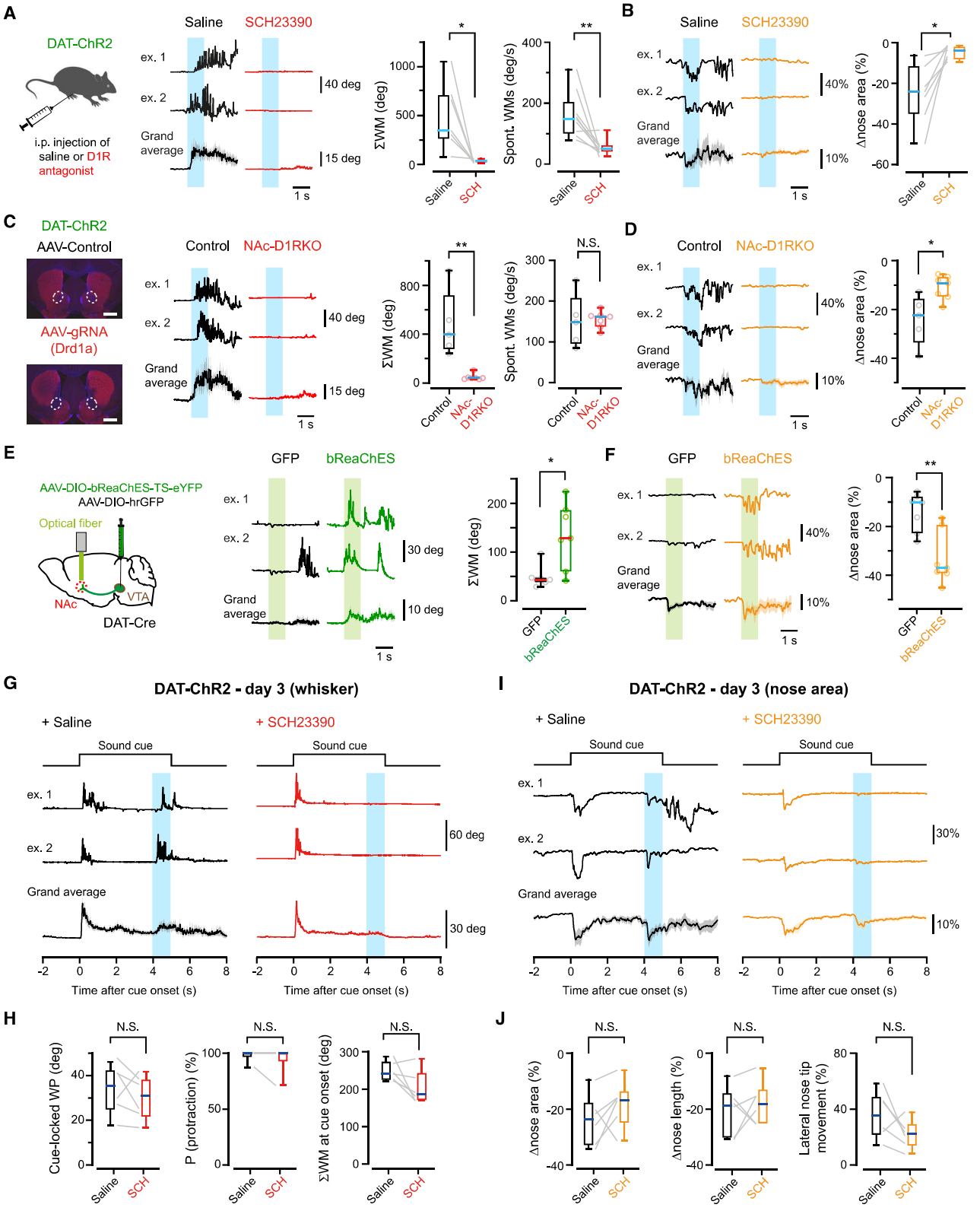

Figure 4. Essential involvement of accumbal D1Rs in oDAS-induced orofacial movements

(A) Left, schematic for the experiment. Middle, example and grand average traces of the whisker position upon oDAS (light blue shadow) in trials with i.p. injection of SCH23390 (red) and saline (black) (n = 7 mice). Right, ΣWM during oDAS and the magnitude of spontaneous WMs (Spont. WMs, n = 9 mice).

(legend continued on next page)

pairing for 2 days and analyzed orofacial movements upon the paired stimulation on the third day. Even with the potent effects of SCH23390 on spontaneous and oDAS-induced motions (Figure 4A), it did not affect the cue-locked WP (amplitude: saline = 33.8° ± 4.4° [n = 6 mice], SCH23390 = 30.0° ± 4.0° [n = 6 mice], p = 0.35, paired t test) (Figures 4G and 4H). The D1R antagonist did also not significantly attenuate nose twitches time-locked to the sound cue (Δnose area: saline = 24.0° ± 3.7° [n = 6 mice], SCH23390 = 18.3° ± 3.4° [n = 6 mice], p = 0.20, paired t test) (Figures 4I and 4J). Thus, the oDAS-induced and cue-locked orofacial movements are differentially driven by D1R-dependent and -independent neuronal mechanisms, respectively. An i.p. injection of SCH23390 together with a D2 receptor (D2R) antagonist, raclopride (3 mg/kg), did not affect cue-locked WMs (Figures S4F and S4G), but it largely attenuated the cue-locked nose movements (Figures S4H and S4I), suggesting that distinct mechanisms regulate whisker and nose movements time-locked to reward-predicting cue presentation.

Whisker M1 facilitates uninstructed orofacial movements

Mouse wM1 plays a critical role in triggering exploratory whisking.[30–32] We next examined the involvement of wM1 in oDAS-induced orofacial movements. Silencing of wM1 by injection of muscimol (5 mM in Ringer's solution, total 400 nL), a $GABA_A$-receptor agonist, led to a dramatic drop in the magnitude and probability of oDAS-induced WMs (ΣWM: before muscimol = 243° ± 40° [n = 6 mice], after muscimol = 55.0° ± 12.0° [n = 6 mice], p = 0.0095, paired t test; whisking probability: before muscimol = 59.9 ± 6.1% [n = 6 mice], after muscimol = 17.1 ± 6.4% [n = 6 mice], p = 0.0027, paired t test) (Figures 5A and 5B). Inactivation of wM1 by muscimol also attenuated oDAS-induced nose twitches (Δnose area: before muscimol = 24.2 ± 1.6% [n = 6 mice], after muscimol = 5.6 ± 1.3% [n = 6 mice], p = 0.0001, paired t test; Figures 5C, 5D, and S5A). Injection of Ringer's solution in wM1 did not affect these oDAS-induced orofacial movements (Figures 5C, 5D, and S5A). Thus, neuronal activity in wM1 is required for the generation of oDAS-induced orofacial movements.

We further investigated whether the cue-locked orofacial movements during the sound-oDAS pairing stimuli also depend on wM1 activity. We used DAT-ChR2 mice that learned the sound-oDAS pairing for 2–4 days and tested injection of muscimol or Ringer's solution into wM1 on the next day. Inactivation of wM1 by muscimol largely attenuated the cue-locked WP (amplitude: before muscimol = 25.8° ± 4.0° [n = 6 mice], after muscimol = 4.6° ± 1.4° [n = 6 mice], p = 0.031, Wilcoxon signed rank test; probability: before muscimol = 95.8 ± 2.7% [n = 6 mice], after muscimol = 22.7 ± 8.5% [n = 6 mice], p = 0.031, Wilcoxon signed rank test; Figures 5E, 5F, and S5B) and nose twitch (Δnose area: before muscimol = 24.0 ± 5.2% [n = 6 mice], after muscimol = 6.5 ± 1.7% [n = 6 mice], p = 0.013, paired t test; Figures 5G, 5H, and S5C). Injection of Ringer's solution did not affect the cue-locked orofacial movements (Figures 5G, 5H, and S5C). Our results thus suggest that wM1 activity is crucial for the generation of both oDAS-induced and cue-locked orofacial movements.

Representation of uninstructed orofacial movements in wM1

wM1 thus appears to play a pivotal role in orchestrating uninstructed orofacial movements, which led us to investigate the neuronal signals within this region during these movements. Using multisite silicone probes, we measured the action potential firing in the wM1 of head-restrained DAT-ChR2 mice during sound-oDAS pairing stimulation. We performed recordings in four DAT-ChR2 mice that had already experienced the sound-oDAS pairing conditioning for 3 days. The orofacial behaviors of these mice on the recording day were essentially the same as those on day 2 (Figures S6A and S6B). Among the 174 units we identified, 103 units (59.2%) significantly increased or decreased their firing rate at the cue onset and/or during oDAS. To examine the correlation between the activity of individual neurons and whisker behavior, we first categorized trials based on the behavior (Figures 6A and 6B). In 20.8% of trials, both cue-locked WP and whisking during oDAS were observed ("CL + OA trials", n = 4 mice). There were also trials with only Cue-WP but not oDAS-aligned WMs ("CL trials", 37.6%) and those with only oDAS-aligned WMs but not Cue-WP ("OA trials", 11.9%). We next analyzed the correlation between the firing rates of each neuron and whisker behaviors in these trials. We found that the neurons specifically representing cue-locked motion ("CL cells") showed a correlation of their

(B) Example and grand average traces (left) and quantifications (right) of the top-view nose area in trials with i.p. injection of saline (black) or SCH23390 (orange) (n = 7 mice).
(C) Left, epifluorescence images of coronal sections containing NAc (dashed circles) from mice with bilateral injection of AAV with guide RNA targeting *Drd1a* (bottom) or control AAV with shuffled RNA (top). Red, Drd1 immunoreactivity; blue, DAPI. Scale bars, 1 mm. Middle, example and grand average traces of the whisker position in NAc-D1R-KO (red) and control (black) mice upon oDAS. Right, ΣWM and the magnitude of Spont. WMs during oDAS. Control, n = 5 mice; NAc-D1R-KO, n = 7 mice.
(D) Same as (B) but for data from NAc-D1R-KO (orange) and control (black) mice.
(E) Left, schematic for the optogenetic experiment. Middle, example and grand average traces of the whisker position upon oDAS in bReaChES- (green) and GFP- (black) expressing mice. Right, data for each mouse (thin lines) and boxplots for the ΣWM during oDAS (n = 7 mice for each).
(F) Same as (B) but for data from bReaChES- (orange) and GFP- (black) expressing mice. Green shadow, stimulation timing.
(G) Example and grand average traces of the whisker position in trials with i.p. injection of SCH23390 (red) or saline (black) in DAT-ChR2 mice during sound-oDAS pairing experiments on day 3 (n = 6 mice). The timings of the sound cue presentation (black line) and oDAS (light blue shadow) are indicated.
(H) Quantification of cue-locked WP and WM with SCH23390 or saline injection.
(I) Same as (G) but for traces of the nose area with i.p. injection of SCH23390 (orange) or saline (black).
(J) Same as (H) but for the parameters of cue-locked nose movements.
Medians of the boxplots are shown in magenta or cyan. Shadows of grand average traces, ± SEM. Open circles and lightly colored lines correspond to individual data. **p < 0.01, *p < 0.05; N.S., not significant; paired t test in (A) and (B), Cue-locked WP and ΣWM in (H) and (J), Mann-Whitney *U* test in ΣWM in (C) and (E), and P (protraction) in (H) or unpaired t test (Spont. WMs in C and D).
See also Figure S4.

CellPress
OPEN ACCESS

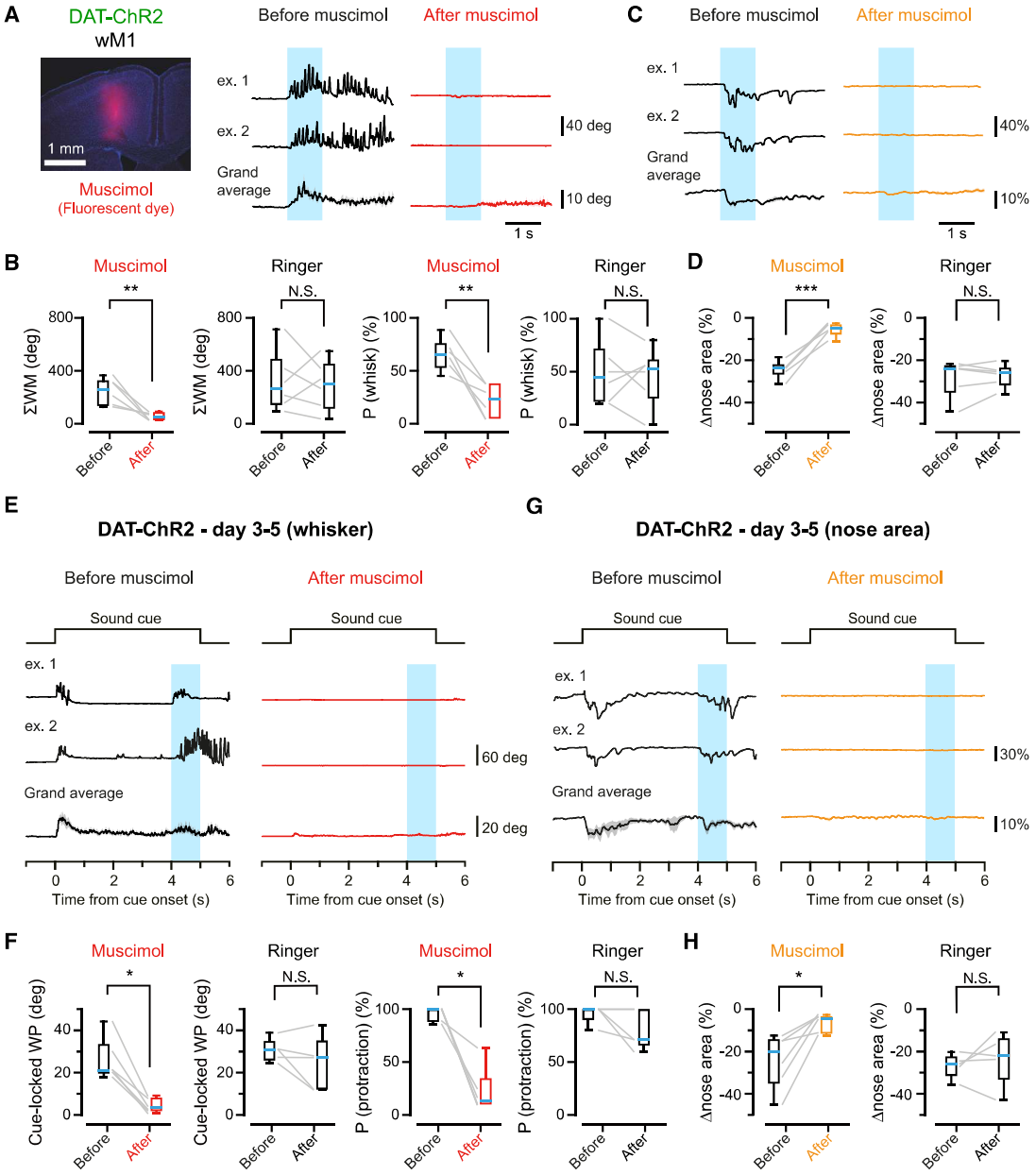

Figure 5. Dominant role of wM1 in driving reward-related orofacial movements

(A) Left, an epifluorescence image of a coronal section indicating the muscimol injection site. A small volume of Chicago sky blue (red) was dissolved into the vehicle. Blue, DAPI (right); example and grand average traces of the whisker position upon oDAS (light blue shadow) before (black) and after (red) muscimol injection in wM1 of DAT-ChR2 mice (n = 6 mice).

(B) ΣWM and the probability of whisking initiation in trials before (black) and after (red) injection of muscimol or Ringer's solution (n = 6 mice for each).

(C) Example and grand average traces of the nose area before (black) and after (orange) muscimol injection into wM1.

(D) Same as (B) but for the change in the nose area.

(E) Example and grand average traces of the whisker position before (black) and after (red) muscimol injection into wM1 of DAT-ChR2 mice during sound-oDAS pairing experiments.

(F) Same as (B) but for the amplitude and occurrence probability of cue-locked WP during sound-oDAS pairing experiments. Ringer, n = 5 mice; muscimol, n = 6 mice.

(G and H) Same as (E) and (F) but for the change in the nose area.

Medians of the boxplots are shown in cyan. Thin lines correspond to individual data. Shadows of grand average traces, ±SEM. ***$p < 0.001$, **$p < 0.01$, *$p < 0.05$; N.S., not significant; paired t test (all of B, D, and H, and cue-locked WP for Ringer in F) or Wilcoxon signed rank test (two panels for muscimol and P [protraction] for Ringer in F).

See also Figure S5.

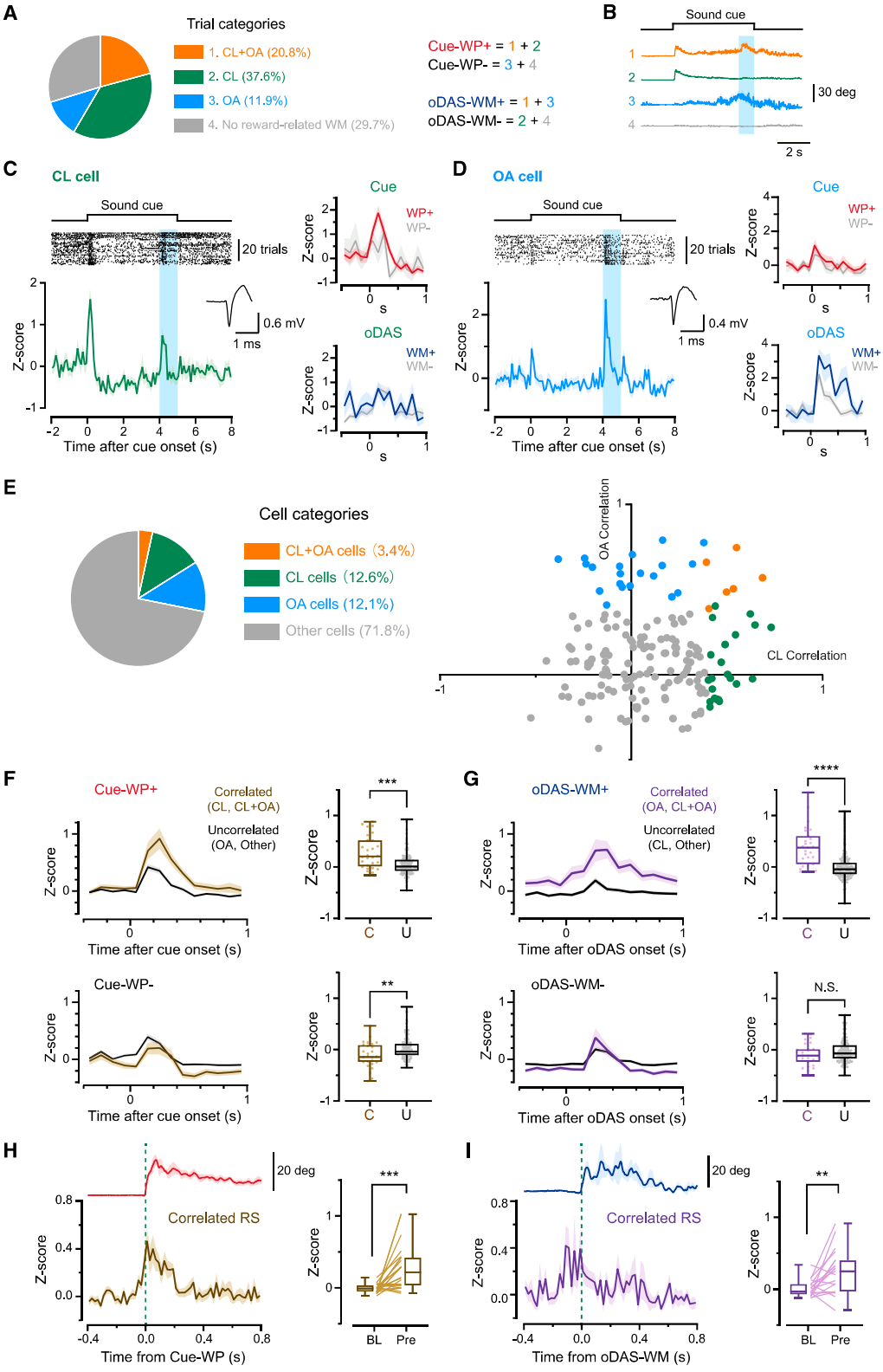

Figure 6. Neuronal representation of cue-locked and oDAS-induced whisker movements in wM1

(A) Summary of the trial categories. CL, trials with cue-locked WP (Cue-WP); OA, trials with WMs during oDAS (oDAS-WM); CL + OA, trials with both Cue-WP and oDAS-WM; +, with motion; –, without motion.

(legend continued on next page)

firing rates at the cue onset with the amplitudes of WP without correlating with WMs during oDAS (Figures 6C and S6C). In contrast, neurons representing oDAS-aligned motion ("OA cells") showed firings correlated with oDAS-aligned motion but not with the cue-locked motion (Figures 6D and S6C). In addition, a subset of wM1 units represented both types of WM ("CL + OA cells"; Figures 6E and S6C). In our recordings, 12.6% of the units were classified as CL cells, 12.1% as OA cells, and 3.4% as CL + OA cells (Figure 6E). We also analyzed the correlation between the cellular activities in wM1 and nose movements (nose area), finding that only 2.3% of wM1 cells are significantly correlated only with the nose (but not whisker) movement. In contrast, wM1 contained 20.1% of cells whose firings are correlated specifically with whisker motion (either cue-locked or oDAS-aligned or both of them) and not with nose motion (Figures S6D and S6E). These results suggest that the wM1 region we studied is more implicated in WMs than nose movements.

In wM1, these cells with correlated firings to each type of whisker motion increased firing rates during the corresponding motion type than uncorrelated cells but not in trials without movements (Figures 6F and 6G). We further separated units into regular spiking (RS) and fast spiking (FS) units, according to their trough-to-peak time of average spike waveform (Figure S7A). We found no apparent specificity in the fraction of FS cells in these CL and OA cells (Figures S7B and S7C) and other stimulus-modified neurons (Figure S7D). The RS cells correlated with cue-locked or oDAS-aligned WMs showed an increase in spike rates slightly before or at around the motion onset (Figures 6H and 6I). Our results thus suggest that wM1 contains specific neuronal populations that facilitate the initiation of stereotyped uninstructed WMs at the timings of reward expectation and acquisition.

Stimulation of wM1 triggers whisker and nose movements

wM1 may be a circuit node that channels signals related to reward expectation and acquisition to facilitate distinct orofacial movements. If this hypothesis is true, stimulating wM1 should result in orofacial movements with a shorter onset latency than those observed after oDAS or the reward cue presentation. Therefore, we investigated the onset latency with which stimulation of wM1 could induce orofacial movements. To express ChR2 in wM1 neurons, we administered AAV (AAV9-CaMKII-ChR2-mCherry) injections in wM1 (Figure 7A). After 4–5 weeks of expression, we delivered blue light pulses using the same protocol as our strongest oDAS (5 ms, 20 times at 20 Hz) to the wM1, which led to whisking and nose twitches with shorter average latencies than oDAS (Figures 7B and 7C). In control mice with virally induced expression of mCherry in wM1, blue light stimulation did not evoke whisker and nose movements (mCherry vs. ChR2, n = 6 for each; ΣWM: 47.8° ± 4.8° vs. 1,176° ± 113°, $p < 0.0001$, unpaired t test; whisking probability: 3.9 ± 2.5% vs. 100 ± 0%, $p = 0.0022$, Mann-Whitney *U* test; Δnose area: 9.2 ± 2.0% vs. 27.4 ± 5.0%, $p = 0.0070$, unpaired t test; Δnose length: 7.1 ± 1.7% vs. 22.1 ± 4.5%, $p = 0.011$, unpaired t test; lateral nose tip movement: 7.6 ± 1.2% vs. 38.7 ± 6.3%, $p = 0.0007$, unpaired t test). We also tested transient stimulation of wM1 neurons with a brief high-frequency train of blue light pulses (5 ms, 4 times at 100 Hz), which resulted in transient whisker and nose movements resembling cue-locked orofacial movements (Figures 7D and 7E). The average latencies of wM1-driven transient whisker and nose movements were significantly shorter than those of cue-locked movements (Figures 7D and 7E). Thus, wM1-driven orofacial movements exhibited shorter onset latencies than orofacial movements after cue presentation or oDAS. Next, we explored whether wM1 stimulation could replicate certain aspects of orofacial movements. WMs induced by sustained stimulation (1 s, 20 Hz, 20 times) exhibited greater vigor and duration compared with those induced by transient stimulation (100 Hz, 4 times), differentiable through a machine-learning model based on WP amplitude and ΣWM (Figure 7F). Our model successfully distinguished wM1-driven transient WMs from oDAS-induced motion (Figure 7G). However, the models were unable to differentiate between wM1-driven transient WMs and cue-locked WMs (Figure 7G). Through various stimulation protocols on wM1, we discovered a specific pattern involving 5-ms pulses at 50 Hz for 25 times that induced WMs akin to oDAS-induced but not cue-locked motion (Figure 7G). These results suggest that wM1 stimulation with different patterns can effectively elicit orofacial movements similar to those observed during the sound-oDAS pairing task.

(B) Grand average traces of the whisker position in trial categories indicated in (A).
(C) Left, example raster plot (top) and corresponding *Z* scored peri-stimulus time histogram (PSTH, bottom) obtained from a representative CL cell. The averaged action potential waveform is shown in the inset. Right, *Z* scored PSTH of the same cell at around the cue onset (top) and upon oDAS (bottom), comparing data with (+) or without (−) Cue-WP or oDAS-WM.
(D) Same as (C) but for a representative OA cell.
(E) Left, summary of the cell categories. Right, scatterplot containing 174 neurons from four mice experiencing the sound-oDAS pairing stimulation on the fourth day of conditioning, plotted on the basis of their correlation to the ΣWM during oDAS (OA correlation) and the Cue-WP amplitude (CL correlation). Subsets of neurons showing significant, positive correlation are colored in orange (CL + OA cell), green (CL cell), or cyan (OA cell).
(F) Left, average *Z* scored PSTHs of Cue-WP-correlated (C) and -uncorrelated (U) cells at around the cue onset, comparing data with (+, top) or without (−, bottom) Cue-WP. Right, average *Z* scored firing rates at 0–1 s after the cue onset.
(G) Same as (F) but for oDAS-WM-correlated (C) and -uncorrelated (U) cells upon oDAS.
(H) Left, *Z* scored average PSTHs of Cue-WP-correlated RS cells (n = 24 cells) and corresponding grand-averaged whisker positions (n = 4 mice) aligned at the motion onset. Right, averaged *Z* score of firing rates at baseline (BL, 0.2–0.4 s before the onset) and pre-motion (Pre, 0.04–0 s before the onset).
(I) Same as (H) but for oDAS-WM-correlated RS cells (n = 21 cells, 4 mice) upon oDAS.
A thick line and shadows indicate mean ± SEM. ****$p < 0.0001$, ***$p < 0.001$, **$p < 0.01$; N.S., not significant; Mann-Whitney *U* test in (F) and (G) or Wilcoxon signed rank test in (H) and (I).
See also Figures S6 and S7.

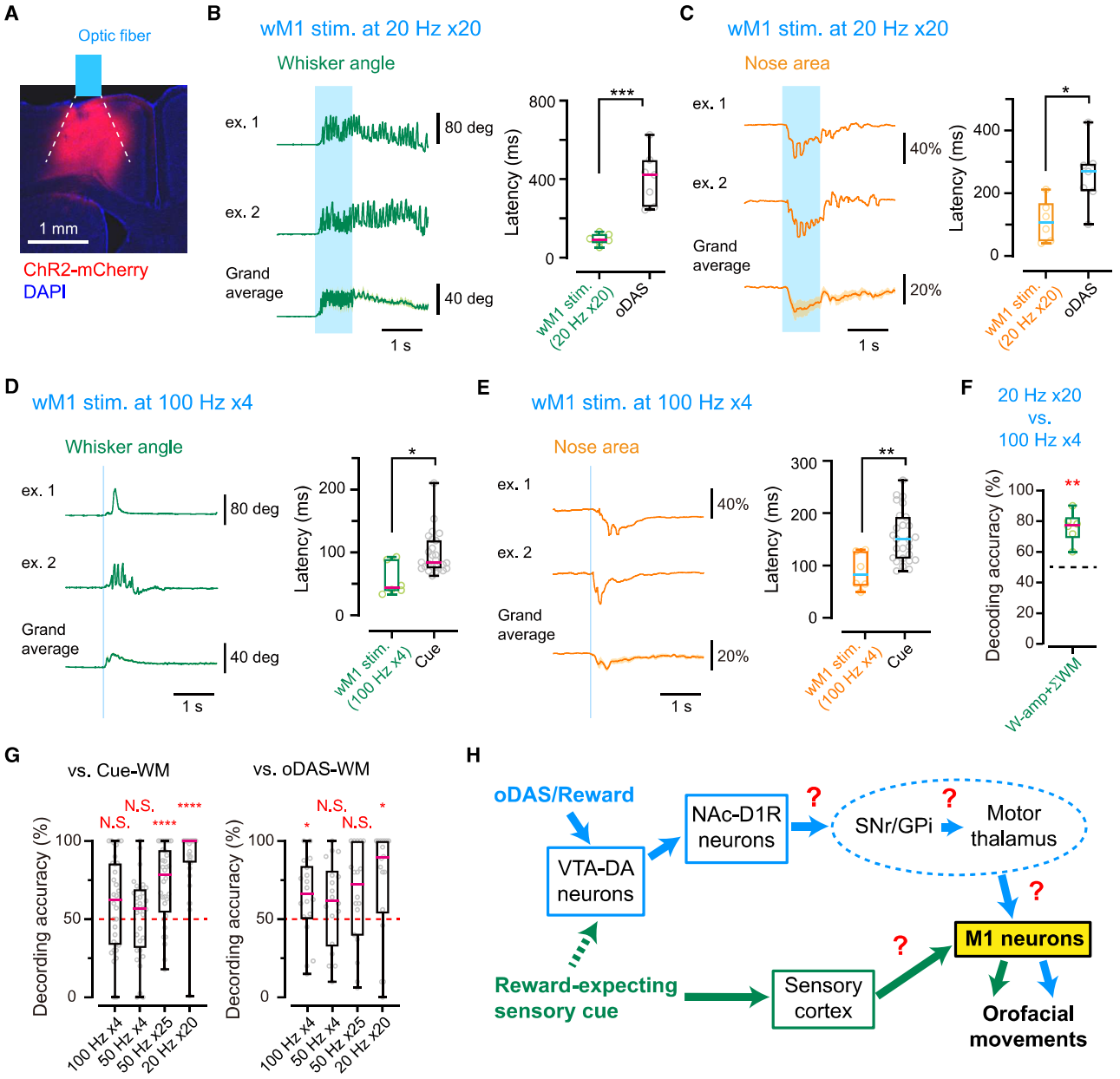

Figure 7. Optogenetic stimulation of wM1 induced whisker and nose movements

(A) An epifluorescence image of a coronal section indicating the AAV injection site at wM1. A schematic of the range of blue light illumination (dotted lines) with an optic fiber is superimposed.

(B) Left, example and grand average traces of the whisker position upon photostimulation (5 ms, 20 pulses at 20 Hz) of wM1 expressing ChR2 (n = 6 mice). Right, onset latency of the WM upon wM1 photostimulation and oDAS (same data as Figure 2J, 20 Hz ×20).

(C) Same as (B) but for the nose area (left) and the onset of nose movement (right).

(D) Same as (A) but with a transient wM1 photostimulation (5 ms, 4 pulses at 100 Hz; n = 6 mice). The onset latency of whisker movements is compared with that of the cue-locked movements (same data as Figure 3G, D2).

(E) Same as (C) but with the transient stimulation.

(F) Decoding accuracy by a model based on the WP amplitude (W-amp) and ΣWM to discriminate between wM1 stimulation with 20 pulses at 20 Hz and that with 4 pulses at 100 Hz.

(G) Decoding accuracies by models based on W-amp and ΣWM for distinguishing wM1-driven WMs with different stimulus protocols and those at the cue onset of the sound-oDAS task on day 2 (left, Cue-WM) or during oDAS (right, oDAS-WM).

(H) Schematic of presumable neural circuits for triggering uninstructed orofacial movements. SNr, substantia nigra pars reticulata; GPi, globus pallidus interna. Medians of the boxplots are shown in cyan. Shadows of grand average traces, ±SEM. Open circles correspond to individual data.****$p < 0.0001$, **$p < 0.01$, *$p < 0.05$; N.S., not significant; unpaired t test in (B), (C), and (F), Mann-Whitney *U* test in (D), or one-sample t test vs. the chance level (50%) in (F) and (G), except for 50 Hz ×25 and 20 Hz ×20 vs. Cue-WM and 20 Hz ×20 vs. oDAS-WM in (G) with one-sample Wilcoxon test.

DISCUSSION

Through high-speed filming of orofacial movements of head-restrained mice performing reward-based learning tasks, we have characterized uninstructed facial movements at the timings of expectation and acquisition of a reward. Previous studies showing task-aligned uninstructed orofacial movements[5–8,10–13] used tasks involving motor actions for execution, such as holding handles, locomotion, and licking. The uninstructed orofacial motions during a task typically occur along with goal-directed actions. Using a Pavlovian learning paradigm, however, we demonstrated that uninstructed orofacial movements would become task-aligned even without any need for motor action.

WP time-locked to the reward-predicting cue presentation could be elicited in multiple reward-based tasks. The mean amplitude of the cue-locked WP increased as the mice learned the tasks. Such generality and scalability of the behavior suggest that it may not merely be a reflexive movement upon sensory stimuli but rather influenced by the expectation of obtaining a reward.[12,14,15] A quick nose twitch is often coupled to the cue-locked WP. These highly reproducible cue-locked orofacial movements appeared only transiently, followed by more random orofacial movements at the later phases of the cue presentation. Our observations are in line with the studies showing increased body and facial activities, including enhanced locomotion and sniffing at a higher frequency upon reward expectation.[12,43–46]

The oDAS-induced whisker motions have longer latency, are more persistent than the cue-locked WP, and generally have a protracted set point, similar to exploratory whisking[30–32] as well as active whisking upon water reward, except for licking-associated oscillatory movements (Figure 3J). Nose twitches also accompany the oDAS-induced WMs, suggesting the occurrence of sniffing.[44,47] The oDAS-induced WM displays scalable positive relationships with the stimulus frequency and intensity, indicating a connection to reward-prediction error signals.[19,26–28,48] We speculate that the oDAS-induced orofacial movements could potentially serve as a mechanism for gathering environmental sensory information, thereby leading to rewarding experiences. Alternatively, these orofacial movements may function as perceptible signals of internal states, potentially communicated to conspecifics via social facial touches.

WMs are driven by facial muscles innervated by cholinergic motor neurons in the lateral facial nucleus. These whisker motor neurons receive synaptic inputs from distributed premotor neurons in the brain stem, the midbrain, and the neocortex.[49,50] Our studies suggest that VTA-DA neurons could directly or indirectly regulate these circuits, possibly via an accumbal D1Rs-dependent mechanism. D1R-expressing GABAergic neurons in the NAc (NAc-D1R neurons), projecting to the substantia nigra pars reticulata (SNr), can initiate a signal flow resulting in activation of motor-related nuclei of the thalamus (motor thalamus) and wM1. wM1 neurons innervate brain stem reticular nuclei containing whisker premotor neurons,[30,31] potentially forming a central pattern generator for rhythmic whisking.[17,51] Such signal transmission from VTA to whisker premotor neurons through wM1 might facilitate the uninstructed orofacial movements in mice (Figure 7H). However, we cannot exclude the possibility that signals from NAc-D1R neurons through pathways independent of wM1 might also contribute to the activation of motor neurons in the facial nucleus.

The transient WPs upon reward-predicting cues are reminiscent of transient firings of VTA-DA neurons and subsequent DA release in the NAc immediately after reward-predicting cue presentation.[26–28,52] As discussed above, DA released in the NAc would activate D1R-expressing neurons,[41] generating the signal flow toward wM1. However, D1Rs do not mediate the cue-locked orofacial movements (Figures 4G–4J). The latency of cue-locked WP (~100 ms) is much faster than oDAS-induced motion (~400 ms). Therefore, learning a stimulus-reward association might recruit a cortical sensorimotor-coupling for reward expectation signaling, thereby activating wM1 earlier than the signals through NAc-D1R neurons. Transient stimulation of wM1 could evoke transient WMs with protraction, similar to but with a shorter latency than the cue-locked movements (Figures 7D and 7G). The oDAS-induced and cue-locked movements are thus likely driven by different signal pathways: the oDAS-induced movements are dependent on NAc-D1Rs, while cue-locked movements are not; however, both signals converge into wM1 (Figure 7H).

Our findings provided insights into the neuronal mechanisms of uninstructed, task-aligned orofacial movements. We found that different neuronal populations in the wM1 area signal cue-locked, transient WPs and oDAS-aligned, active whisking. This finding supports previous studies[32,34,36] that indicate different cells within the wM1 represent various aspects of WMs. Given the strong correlation between orofacial movements and brain-wide neuronal activity,[4–7,9] it is likely that the activity of these wM1 neurons not only contributes to orofacial movements during reward-based behaviors but also has a broader impact on overall brain processing.

STAR★METHODS

Detailed methods are provided in the online version of this paper and include the following:

- KEY RESOURCES TABLE
- RESOURCE AVAILABILITY
  - Lead contact
  - Materials availability
  - Data and code availability
- EXPERIMENTAL MODEL AND SUBJECT DETAILS
  - Animals
  - Cell lines
  - Experimental design
- METHOD DETAILS
  - Plasmids
  - Viral production
  - Heteroduplex cleavage assay
  - Animal preparation and surgery
  - Behavioral tasks
  - Optogenetics
  - Pharmacological perturbation
  - Immunostaining
  - Electrophysiology
- QUANTIFICATION AND STATISTICAL ANALYSIS
  - Motion energy analysis

- Analysis of whisker movements
- Analysis of nose movements
- Machine learning models
- Classification of single units
- Analysis of the correlation between spike rates and whisker behavior
- Statistics

SUPPLEMENTAL INFORMATION

Supplemental information can be found online at https://doi.org/10.1016/j.cub.2023.07.013.

ACKNOWLEDGMENTS

We thank Dr. H. Kasai for providing DAT-IRES-Cre mice Dr. K. Ono for providing Ai32 mice; Dr. K. Deisseroth for providing bReaChES plasmid; Drs. T. Hikida, Y. Ohmura, and J. Dijkstra for discussion; J. Ozaki for collaboration at the early phase of the study; N. Fukatsu for helping with nose analysis; E. Charrière, S. Tsukamoto, A. Kambara, M. Jin, and E. Imoto for technical assistance. This work was supported by JSPS KAKENHI grants (17H05744, 18K19496, 21H00215, and 23H04685) and JST FOREST Program (JPMJFR204H) to T.Y.; research grants from Naito Foundation, Takeda Science Foundation, and Fujita Health University to T.Y.; and JNNS30 Commemorative Research Grant to J.Y.

AUTHOR CONTRIBUTIONS

W.-R.L., T.N., K.M., J.Y., and T.Y. designed the study. W.-R.L., K.M., M.K., T.M., Y.M., and T.Y. performed experiments and analyzed data. T.N. and J.Y. developed machine-learning algorithms and analyzed data. T.D. developed MATLAB codes for motion energy analysis. A.Y. provided plasmids and AAVs and contributed to interpreting the results. H.I. and H.A. provided plasmids for *in vivo* genome editing, performed pilot experiments, and contributed to interpreting the results. T.Y. and C.C.H.P. contributed to data collection related to the whisker detection task. W.-R.L. and T.Y. drafted and wrote the manuscript, with input from other co-authors.

DECLARATION OF INTERESTS

The authors declare no competing interests.

INCLUSION AND DIVERSITY

We support inclusive, diverse, and equitable conduct of research.

Received: June 11, 2023
Revised: July 6, 2023
Accepted: July 10, 2023
Published: August 2, 2023

REFERENCES

1. Busse, L., Cardin, J.A., Chiappe, M.E., Halassa, M.M., McGinley, M.J., Yamashita, T., and Saleem, A.B. (2017). Sensation during active behaviors. J. Neurosci. *37*, 10826–10834. https://doi.org/10.1523/JNEUROSCI.1828-17.2017.
2. Niell, C.M., and Scanziani, M. (2021). How cortical circuits implement cortical computations: mouse visual cortex as a model. Annu. Rev. Neurosci. *44*, 517–546. https://doi.org/10.1146/annurev-neuro-102320-085825.
3. Avitan, L., and Stringer, C. (2022). Not so spontaneous: Multi-dimensional representations of behaviors and context in sensory areas. Neuron *110*, 3064–3075. https://doi.org/10.1016/j.neuron.2022.06.019.
4. Stringer, C., Pachitariu, M., Steinmetz, N., Reddy, C.B., Carandini, M., and Harris, K.D. (2019). Spontaneous behaviors drive multidimensional, brain-wide activity. Science *364*, 255. https://doi.org/10.1126/science.aav7893.
5. Musall, S., Kaufman, M.T., Juavinett, A.L., Gluf, S., and Churchland, A.K. (2019). Single-trial neural dynamics are dominated by richly varied movements. Nat. Neurosci. *22*, 1677–1686. https://doi.org/10.1038/s41593-019-0502-4.
6. Steinmetz, N.A., Zatka-Haas, P., Carandini, M., and Harris, K.D. (2019). Distributed coding of choice, action and engagement across the mouse brain. Nature *576*, 266–273. https://doi.org/10.1038/s41586-019-1787-x.
7. Salkoff, D.B., Zagha, E., McCarthy, E., and McCormick, D.A. (2020). Movement and performance explain widespread cortical activity in a visual detection task. Cereb. Cortex *30*, 421–437. https://doi.org/10.1093/cercor/bhz206.
8. Tremblay, S., Testard, C., DiTullio, R.W., Inchauspé, J., and Petrides, M. (2023). Neural cognitive signals during spontaneous movements in the macaque. Nat. Neurosci. *26*, 295–305. https://doi.org/10.1038/s41593-022-01220-4.
9. Bimbard, C., Sit, T.P.H., Lebedeva, A., Reddy, C.B., Harris, K.D., and Carandini, M. (2023). Behavioral origin of sound-evoked activity in mouse visual cortex. Nat. Neurosci. *26*, 251–258. https://doi.org/10.1038/s41593-022-01227-x.
10. Sachidhanandam, S., Sreenivasan, V., Kyriakatos, A., Kremer, Y., and Petersen, C.C.H. (2013). Membrane potential correlates of sensory perception in mouse barrel cortex. Nat. Neurosci. *16*, 1671–1677. https://doi.org/10.1038/nn.3532.
11. Esmaeili, V., Tamura, K., Muscinelli, S.P., Modirshanechi, A., Boscaglia, M., Lee, A.B., Oryshchuk, A., Foustoukos, G., Liu, Y., Crochet, S., et al. (2021). Rapid suppression and sustained activation of distinct cortical regions for a delayed sensory-triggered motor response. Neuron *109*, 2183–2201.e9. https://doi.org/10.1016/j.neuron.2021.05.005.
12. Dominiak, S.E., Nashaat, M.A., Sehara, K., Oraby, H., Larkum, M.E., and Sachdev, R.N.S. (2019). Whisking asymmetry signals motor preparation and the behavioral state of mice. J. Neurosci. *39*, 9818–9830. https://doi.org/10.1523/JNEUROSCI.1809-19.2019.
13. Coddington, L.T., Lindo, S.E., and Dudman, J.T. (2023). Mesolimbic dopamine adapts the rate of learning from action. Nature *614*, 294–302. https://doi.org/10.1038/s41586-022-05614-z.
14. Dolensek, N., Gehrlach, D.A., Klein, A.S., and Gogolla, N. (2020). Facial expressions of emotion states and their neuronal correlates in mice. Science *368*, 89–94. https://doi.org/10.1126/science.aaz9468.
15. Deschênes, M., Moore, J., and Kleinfeld, D. (2012). Sniffing and whisking in rodents. Curr. Opin. Neurobiol. *22*, 243–250. https://doi.org/10.1016/j.conb.2011.11.013.
16. Welzl, H., and Bureš, J. (1977). Lick-synchronized breathing in rats. Physiol. Behav. *18*, 751–753. https://doi.org/10.1016/0031-9384(77)90079-8.
17. Moore, J.D., Deschênes, M., Furuta, T., Huber, D., Smear, M.C., Demers, M., and Kleinfeld, D. (2013). Hierarchy of orofacial rhythms revealed through whisking and breathing. Nature *497*, 205–210. https://doi.org/10.1038/nature12076.
18. Kurnikova, A., Moore, J.D., Liao, S.M., Deschênes, M., and Kleinfeld, D. (2017). Coordination of orofacial motor actions into exploratory behavior by rat. Curr. Biol. *27*, 688–696. https://doi.org/10.1016/j.cub.2017.01.013.
19. Schultz, W., Dayan, P., and Montague, P.R. (1997). A neural substrate of prediction and reward. Science *275*, 1593–1599. https://doi.org/10.1126/science.275.5306.1593.
20. Berridge, K.C., and Robinson, T.E. (1998). What is the role of dopamine in reward: hedonic impact, reward learning, or incentive salience? Brain Res. Rev. *28*, 309–369. https://doi.org/10.1016/S0165-0173(98)00019-8.
21. Berridge, K.C., and Kringelbach, M.L. (2015). Pleasure systems in the brain. Neuron *86*, 646–664. https://doi.org/10.1016/j.neuron.2015.02.018.
22. Tsai, H.C., Zhang, F., Adamantidis, A., Stuber, G.D., Bonci, A., de Lecea, L., and Deisseroth, K. (2009). Phasic firing in dopaminergic neurons is

sufficient for behavioral conditioning. Science *324*, 1080–1084. https://doi.org/10.1126/science.1168878.

23. Adamantidis, A.R., Tsai, H.C., Boutrel, B., Zhang, F., Stuber, G.D., Budygin, E.A., Touriño, C., Bonci, A., Deisseroth, K., and de Lecea, L. (2011). Optogenetic interrogation of dopaminergic modulation of the multiple phases of reward-seeking behavior. J. Neurosci. *31*, 10829–10835. https://doi.org/10.1523/JNEUROSCI.2246-11.2011.
24. Pascoli, V., Hiver, A., Van Zessen, R., Loureiro, M., Achargui, R., Harada, M., Flakowski, J., and Lüscher, C. (2018). Stochastic synaptic plasticity underlying compulsion in a model of addiction. Nature *564*, 366–371. https://doi.org/10.1038/s41586-018-0789-4.
25. Burgess, C.P., Lak, A., Steinmetz, N.A., Zatka-Haas, P., Bai Reddy, C., Jacobs, E.A.K., Linden, J.F., Paton, J.J., Ranson, A., Schröder, S., et al. (2017). High-yield methods for accurate two-alternative visual psychophysics in head-fixed mice. Cell Rep. *20*, 2513–2524. https://doi.org/10.1016/j.celrep.2017.08.047.
26. Cohen, J.Y., Haesler, S., Vong, L., Lowell, B.B., and Uchida, N. (2012). Neuron-type-specific signals for reward and punishment in the ventral tegmental area. Nature *482*, 85–88. https://doi.org/10.1038/nature10754.
27. Tian, J., and Uchida, N. (2015). Habenula lesions reveal that multiple mechanisms underlie dopamine prediction errors. Neuron *87*, 1304–1316. https://doi.org/10.1016/j.neuron.2015.08.028.
28. Starkweather, C.K., Babayan, B.M., Uchida, N., and Gershman, S.J. (2017). Dopamine reward prediction errors reflect hidden-state inference across time. Nat. Neurosci. *20*, 581–589. https://doi.org/10.1038/nn.4520.
29. Brecht, M., Schneider, M., Sakmann, B., and Margrie, T.W. (2004). Whisker movements evoked by stimulation of single pyramidal cells in rat motor cortex. Nature *427*, 704–710. https://doi.org/10.1038/nature02266.
30. Matyas, F., Sreenivasan, V., Marbach, F., Wacongne, C., Barsy, B., Mateo, C., Aronoff, R., and Petersen, C.C.H. (2010). Motor control by sensory cortex. Science *330*, 1240–1243. https://doi.org/10.1126/science.1195797.
31. Sreenivasan, V., Karmakar, K., Rijli, F.M., and Petersen, C.C.H. (2015). Parallel pathways from motor and somatosensory cortex for controlling whisker movements in mice. Eur. J. Neurosci. *41*, 354–367. https://doi.org/10.1111/ejn.12800.
32. Sreenivasan, V., Esmaeili, V., Kiritani, T., Galan, K., Crochet, S., and Petersen, C.C.H. (2016). Movement initiation signals in mouse whisker motor cortex. Neuron *92*, 1368–1382. https://doi.org/10.1016/j.neuron.2016.12.001.
33. Mercer Lindsay, N., Knutsen, P.M., Lozada, A.F., Gibbs, D., Karten, H.J., and Kleinfeld, D. (2019). Orofacial movements involve parallel corticobulbar projections from motor cortex to trigeminal premotor nuclei. Neuron *104*, 765–780.e3. https://doi.org/10.1016/j.neuron.2019.08.032.
34. Hill, D.N., Curtis, J.C., Moore, J.D., and Kleinfeld, D. (2011). Primary motor cortex reports efferent control of vibrissa motion on multiple timescales. Neuron *72*, 344–356. https://doi.org/10.1016/j.neuron.2011.09.020.
35. Friedman, W.A., Zeigler, H.P., and Keller, A. (2012). Vibrissae motor cortex unit activity during whisking. J. Neurophysiol. *107*, 551–563. https://doi.org/10.1152/jn.01132.2010.
36. Gerdjikov, T.V., Haiss, F., Rodriguez-Sierra, O.E., and Schwarz, C. (2013). Rhythmic whisking area (RW) in rat primary motor cortex: an internal monitor of movement-related signals? J. Neurosci. *33*, 14193–14204. https://doi.org/10.1523/JNEUROSCI.0337-13.2013.
37. Yamashita, T., and Petersen, C.C.H. (2016). Target-specific membrane potential dynamics of neocortical projection neurons during goal-directed behavior. eLife *5*, e15798. https://doi.org/10.7554/eLife.15798.
38. Mathis, A., Mamidanna, P., Cury, K.M., Abe, T., Murthy, V.N., Mathis, M.W., and Bethge, M. (2018). DeepLabCut: markerless pose estimation of user-defined body parts with deep learning. Nat. Neurosci. *21*, 1281–1289. https://doi.org/10.1038/s41593-018-0209-y.
39. Dodson, P.D., Dreyer, J.K., Jennings, K.A., Syed, E.C.J., Wade-Martins, R., Cragg, S.J., Bolam, J.P., and Magill, P.J. (2016). Representation of spontaneous movement by dopaminergic neurons is cell-type selective and disrupted in parkinsonism. Proc. Natl. Acad. Sci. USA *113*, E2180–E2188. https://doi.org/10.1073/pnas.1515941113.
40. Howe, M.W., and Dombeck, D.A. (2016). Rapid signalling in distinct dopaminergic axons during locomotion and reward. Nature *535*, 505–510. https://doi.org/10.1038/nature18942.
41. Gunaydin, L.A., Grosenick, L., Finkelstein, J.C., Kauvar, I.V., Fenno, L.E., Adhikari, A., Lammel, S., Mirzabekov, J.J., Airan, R.D., Zalocusky, K.A., et al. (2014). Natural neural projection dynamics underlying social behavior. Cell *157*, 1535–1551. https://doi.org/10.1016/j.cell.2014.05.017.
42. Cui, W., Aida, T., Ito, H., Kobayashi, K., Wada, Y., Kato, S., Nakano, T., Zhu, M., Isa, K., Kobayashi, K., et al. (2020). Dopaminergic signaling in the nucleus accumbens modulates stress-coping strategies during inescapable stress. J. Neurosci. *40*, 7241–7254. https://doi.org/10.1523/JNEUROSCI.0444-20.2020.
43. Bindra, D., and Campbell, J.F. (1967). Motivational effects of rewarding intracranial stimulation. Nature *215*, 375–376. https://doi.org/10.1038/215375a0.
44. Clarke, S., and Trowill, J.A. (1971). Sniffing and motivated behavior in the rat. Physiol. Behav. *6*, 49–52. https://doi.org/10.1016/0031-9384(71)90013-8.
45. Kepecs, A., Uchida, N., and Mainen, Z.F. (2006). The sniff as a unit of olfactory processing. Chem. Senses *31*, 167–179. https://doi.org/10.1093/chemse/bjj016.
46. Saunders, B.T., Richard, J.M., Margolis, E.B., and Janak, P.H. (2018). Dopamine neurons create Pavlovian conditioned stimuli with circuit-defined motivational properties. Nat. Neurosci. *21*, 1072–1083. https://doi.org/10.1038/s41593-018-0191-4.
47. Welker, W.I. (1964). Analysis of sniffing of the albino rat 1). Behaviour *22*, 223–244. https://doi.org/10.1163/156853964X00030.
48. Bayer, H.M., and Glimcher, P.W. (2005). Midbrain dopamine neurons encode a quantitative reward prediction error signal. Neuron *47*, 129–141.
49. Petersen, C.C.H. (2014). Cortical control of whisker movement. Annu. Rev. Neurosci. *37*, 183–203. https://doi.org/10.1146/annurev-neuro-062012-170344.
50. McElvain, L.E., Friedman, B., Karten, H.J., Svoboda, K., Wang, F., Deschênes, M., and Kleinfeld, D. (2018). Circuits in the rodent brainstem that control whisking in concert with other orofacial motor actions. Neuroscience *368*, 152–170. https://doi.org/10.1016/j.neuroscience.2017.08.034.
51. Takatoh, J., Prevosto, V., Thompson, P.M., Lu, J., Chung, L., Harrahill, A., Li, S., Zhao, S., He, Z., Golomb, D., et al. (2022). The whisking oscillator circuit. Nature *609*, 560–568. https://doi.org/10.1038/s41586-022-05144-8.
52. Patriarchi, T., Cho, J.R., Merten, K., Howe, M.W., Marley, A., Xiong, W.H., Folk, R.W., Broussard, G.J., Liang, R., Jang, M.J., et al. (2018). Ultrafast neuronal imaging of dopamine dynamics with designed genetically encoded sensors. Science *360*, eaat4422. https://doi.org/10.1126/science.aat4422.
53. Pachitariu, M., Steinmetz, N.A., Kadir, S.N., Carandini, M., and Harris, K.D. (2016). Fast and accurate spike sorting of high-channel count probes with KiloSort. 30th Conference on Neural Information Processing. In Advances in Neural Information Processing 29 (NIPS 2016), D. Lee, M. Sugiyama, U. Luxburg, I. Guyon, and R. Garnett, eds. (NeurIPS. Proceedings).
54. Madisen, L., Mao, T., Koch, H., Zhuo, J.M., Berenyi, A., Fujisawa, S., Hsu, Y.W., Garcia, A.J., 3rd, Gu, X., Zanella, S., et al. (2012). A toolbox of Cre-dependent optogenetic transgenic mice for light-induced activation and silencing. Nat. Neurosci. *15*, 793–802. https://doi.org/10.1038/nn.3078.
55. Matsubara, T., Yanagida, T., Kawaguchi, N., Nakano, T., Yoshimoto, J., Sezaki, M., Takizawa, H., Tsunoda, S.P., Horigane, S.I., Ueda, S., et al. (2021). Remote control of neural function by X-ray-induced scintillation. Nat. Commun. *12*, 4478. https://doi.org/10.1038/s41467-021-24717-1.

STAR★METHODS

KEY RESOURCES TABLE

REAGENT or RESOURCES	SOURCE	IDENTIFIER
Antibodies		
Anti-GFP, mouse monoclonal	Fujifilm Wako Chemicals	Cat# 012-20461; RRID: AB_664697
Anti-tyrosine hydroxylase, rabbit polyclonal	Merck	Cat# AB152; RRID: AB_390204
Anti-D1R (dopamine receptor-1), guinea pig polyclonal	Frontier Institute	RRID: AB_2571595
CF594-conjugated donkey anti-rabbit IgG	Biotium	Cat# 20152; RRID: AB_10563030
CF488A-conjugated donkey anti-mouse IgG	Biotium	Cat# 20014; RRID: AB_10561327
CF594-conjugated donkey anti-guinea pig IgG	Biotium	Cat# 20170; RRID: AB_10853278
Bacterial and virus strains		
AAV(DJ)-Ef1a-DIO-bReaChES-TS-eYFP	This paper	N/A
AAV9-CMV-DIO-hrGFP	This paper	N/A
AAV9-saCas9-Drd1a-guide RNA	This paper	N/A
AAV9-saCas9-control guide RNA	This paper	N/A
AAV9-Ef1a-DIO hChR2(E123T-T159C)-EYFP	Addgene	Cat# 35509
AAV9-Ef1a-DIO-EYFP	Addgene	Cat# 27056
AAV9-CaMKIIa-hChR2(ET/TC)-mCherry	Addgene	Cat# 35512
AAV9-Ef1a-mCherry	Addgene	Cat# 114470
Chemicals, peptides, and recombinant proteins		
SCH23390 hydrochloride	Merck	Cat# D054
Raclopride tartrate salt	Merck	Cat# R121
Muscimol	Tocris	Cat# 0289
Chicago sky blue 6B	Merck	Cat# C8679
DAPI	Thermo Fisher Scientific	Cat# D1306
BsaI	New England Biolabs	Cat# R0535
T4 DNA ligase	New England Biolabs	Cat# M0202
Benzonase Nuclease	Merck	Cat# 71205
Hank's Balanced Salt Solution (HBSS)	Merck	Cat# H8264
DABCO	Merck	Cat# D27802
Experimental models: Cell lines		
Human: HEK293 cell line	Agilent Scientific Instruments	Cat#240073
Experimental models: Organisms/strains		
Mouse: C57BL/6J wildtype	Japan SLC, Inc.	C57BL/6JJmsSlc
Mouse: C57BL/6J wildtype	Janvier (France)	C57BL/6JRj
Mouse: Slc6a3$^{tm1.1(cre)Bkmn}$/J (DAT-IRES-Cre)	The Jackson Laboratory	RRID: IMSR_JAX: 006660
Mouse: Gt(ROSA)26Sor$^{tm32(CAG-COP4*H134R/EYFP)Hze}$/J (Ai32)	The Jackson Laboratory	RRID: IMSR_JAX:024109
Recombinant DNA		
pAAV-Ef1a-DIO-bReaChES-TS-eYFP	Dr. Karl Deisseroth	N/A
pAAV-CMV-DIO-hrGFP	This paper	N/A
pAAV-saCas9-Drd1a-guide RNA	Cui et al.[42]	N/A
pAAV9-saCas9-control guide RNA	This paper	N/A
Software and algorithms		
ImageJ	NIH	RRID: SCR_002285
GraphPad Prism 9	GraphPad	RRID: SCR_002798
MATLAB	Mathworks	RRID: SCR_001622

(*Continued on next page*)

Continued

REAGENT or RESOURCES	SOURCE	IDENTIFIER
Kilosort	Pachitariu et al.[53]	RRID: SCR_016422
Phy	Pachitariu et al.[53]	https://github.com/cortex-lab/phy
Igor Pro	WaveMetrics	RRID: SCR_000325
DeepLabCut	Mathis et al.[38]	https://github.com/DeepLabCut/DeepLabCut
Python	https://www.python.org/	RRID: SCR_008394
Other		
High-speed camera	Ditect	HAS-L1
470 nm LED	Thorlabs	M470F3
530 nm LED	Thorlabs	M530F2
Optic fiber cannula	Thorlabs	Cat# CFM14L05
Silicon probe	NeuroNexus	A1x32-Poly2-10mm50s-177
Data acquisition system	Open Ephys	Open Ephys Acquisition Board
Vibratome	Leica	VT1000S
Fluorescent microscope	Keyence	BZ-9000
Image viewer for fluorescence microscope	Keyence	BZ-X Viewer
Source data	This paper	https://doi.org/10.5281/zenodo.8119918
Analysis codes	This paper	https://github.com/FHU-DataScience-Group/CurrBiol2023-orofacial-movement

RESOURCE AVAILABILITY

Lead contact

Further information and requests for resources and reagents should be directed to and will be fulfilled by the lead contact, Takayuki Yamashita (takayuki.yamashita@fujita-hu.ac.jp).

Materials availability

This study did not generate new unique reagents.

Data and code availability

All data and analysis codes have been deposited at Zenodo and Github and are publicly available as of the date of publication. DOIs are listed in the key resources table. Any additional information required to reanalyze the data reported in this paper is available from the lead contact upon request.

EXPERIMENTAL MODEL AND SUBJECT DETAILS

Animals

All experimental procedures were approved by the Swiss Federal Veterinary Office (for whisker detection task experiments), the institutional review board of the Research Institute of Environmental Medicine, Nagoya University, and the Institutional Animal Care and Use Committee of Fujita Health University. For optogenetic experiments, we used DAT-ChR2 mice by crossing DAT-IRES-Cre mice [B6.SJL-*Slc6a3*$^{tm1.1(cre)Bkmn}$/J] with Ai32 mice [B6;129S-*Gt(ROSA)26Sor*$^{tm32(CAG-COP4*H134R/EYFP)Hze}$/J],[54] Ai32 mice as control or DAT-IRES-Cre mice with AAV injected (see below). For behavioral experiments using water reward-based learning tasks (Figure 1), we used adult male C57BL/6J wild-type mice. Mice were at least 6-week-old at the time of head-post implantation (see below). Mice were kept in a shifted light/dark cycle (light 0 p.m. to 0 a.m. in Nagoya University and Fujita Health University; light 7 p.m. to 7 a.m. in EPFL) in ventilated cages at a temperature of 23 ± 3°C with food available ad libitum. Behavioral experiments were performed during the dark period. Water was restricted during the training of water reward-based learning tasks. All mice were weighed and inspected daily during behavioral training and given wet food, so that mouse weight was kept to be more than 80% of the initial value.

Cell lines

HEK293 (AAV-293) cell line bought from Agilent (catalog#: 240073) was used for AAV production.

Experimental design

This study did not involve randomization or blinding. We did not estimate the sample size before carrying out the study. However, the sample size in this study is comparable with those used in related studies.[5,11,14,32,55]

METHOD DETAILS

Plasmids

For AAV production, pAAV-Ef1a-DIO-bReaChES-TS-eYFP was obtained from K. Deisseroth (Stanford University). For CRSPR-Cas9-mediated gene editing, we used a plasmid containing a saCas9 encoding sequence with *Drd1a*-targeting short guide RNA[42] (target sequence: 5'-GTATTCCCTAAGAGAGTGGA-3'): pairs of *Drd1a*-targeting oligo DNAs (forward, 5'-CACCGGGTATTCCCTAAGA GAGTGGA-3', reverse, 5'-AAACTCCACTCTCTTAGGGAATACCC-3') were ligated into a plasmid pX601-AAV-CMV::NLS-SaCas9-NLS-3xHA-bGHpA;U6::BsaI-sgRNA (pX601, Addgene #61591) digested with BsaI (R0535, New England BioLabs). We constructed a plasmid with a negative-control saCas9 guide RNA by shuffling bases of the *Drd1a*-targeting guide RNA sequence (target sequence: 5'-TCAATAATGAGGTGGTCCGA-3'): the pX601 was linearized with BsaI, and a pair of oligonucleotides (Forward, 5'-CACCGTCAATAATGAGGTGGTCCGA-3'; Reverse, 5'-AAACTCGGACCACCTCATTATTGAC-3') was ligated with T4 DNA Ligase (M0202, New England BioLabs).

Viral production

To produce AAV vectors for axonal stimulation experiments (Figures 4E and 4F), HEK293 cells were transfected with vector plasmids including pAAV encoding bReaChES or hrGFP together with pHelper, and pAAV-RC (serotype 9 or DJ), using a standard calcium phosphate method. After three days, transfected cells were collected and suspended in lysis buffer (150 mM NaCl, 20 mM Tris pH 8.0). After four freeze-thaw cycles, the cell lysate was treated with 250 U/ml benzonase nuclease (Merck) at 37 °C for 10–15 min with adding 1 mM $MgCl_2$ and then centrifuged at 4 °C at 1753×g for 20 min. AAV was then purified from the supernatant by iodixanol gradient ultracentrifugation. The purified AAV solution was concentrated in PBS via filtration and stored at −80°C.

For *in vivo* genome editing experiment (Figures 4C and 4D), HEK293 cells were transfected with vector plasmids including pAAV encoding *Drd1a*-targeting guide RNA or control guide RNA, together with pHelper, and pAAV-RC (serotype 9), using a standard calcium phosphate method. Transfected cells were collected after three days and suspended in Hank's Balanced Salt Solution (Merck). The AAV-containing cell lysate was treated with 250 U/ml benzonase at 37 °C for 30 min without adding $MgCl_2$, and then centrifuged three times at 17,800×g for 10 min at 4°C with the supernatant after each centrifugation used for the next centrifugation. The final supernatant was then aliquoted and stored at −80°C.

Heteroduplex cleavage assay

To examine the off-target effect of our saCas9-*Drd1a*-gRNA, we performed T7 endonuclease I (T7EI) assay using Alt-R Genome Editing Detection Kit (Integrated DNA Technologies). The saCas9-*Drd1a*-gRNA plasmid or a control hrGFP-expressing plasmid (pAAV-hrGFP Vector, #240074, Agilent) was transfected into NIH/3T3 cells in a 24-well plate using jetOPTIMUS (PolyPlus). After 72 h post-transfection, genomic DNA was isolated using Guide-it Mutation Detection Kit (Takara). DNA fragments flanking the targeted *Drd1a* locus and off-targets (Figure S4C) were then amplified from the purified genomic DNA with PCR. Positive and negative control DNA fragments provided by AltR-Genome Editing Kit were also amplified with PCR. PCR products were denatured and hybridized, digested at 37°C for 60 min with T7EI, and analyzed by electrophoresis in 2% agarose gel stained with ethidium bromide. The gel images were obtained with a transilluminator (E-BOX VX2, Vilber Lourmat).

Animal preparation and surgery

Mice were anesthetized with isoflurane (3.0–3.5% for induction, 1.0–1.5% for maintenance) and head-fixed on a stereotactic device using ear bars or a nose clamp. Body temperature was maintained at ~37°C by a controlled heating pad. An ocular ointment was applied over the eyes to prevent drying. The scalp was cut open to expose the skull. For *in vivo* genome editing (Figures 4C and 4D), AAV harboring *Drd1a*-targeting guide RNA or control guide RNA was bilaterally injected into four sites targeting the NAc (AP: 1 mm, ML: ±1.2 mm, from Bregma, depth: 3.8 mm; and AP: 1.5 mm, ML: ±1.2 mm, from Bregma, depth: 4.0 mm) through small craniotomies (diameter, <~0.5 mm). The injection volume was 500 nl per site. For the experiment with optogenetic axonal stimulation (Figures 4E and 4F), AAV-Ef1a-DIO-bReaChES-TS-eYFP (titer: 6.0×10^{13} copies/ml) or AAV-CMV-DIO-hrGFP (titer: 6.0×10^{12} copies/ml) was injected bilaterally into the VTA (AP: −3.0 mm, ML: ±0.5 mm, from Bregma, depth: 4.2 mm) of DAT-IRES-Cre mice. The injection volume was 200 nl per site. For the experiment with optogenetic stimulation of the SNc-DA neurons (Figures S2E–S2G), AAV9-Ef1a-DIO-hChR2(E123T/T159C)-EYFP (Addgene #35509, obtained from Addgene; the original titer: 2.2×10^{13} copies/ml, diluted to 1/10) or AAV9- Ef1a-DIO-EYFP (Addgene #27056, obtained from Addgene; the original titer: 2.7×10^{13} copies/ml, diluted to 1/10) was injected into the left SNc (AP: -3.1 mm, ML: 1.2 mm, from Bregma, depth: 4.1 mm) of DAT-IRES-Cre mice. The injection volume was 200 nl. For optogenetic stimulation of wM1, AAV9-CaMKIIa-hChR(E123T/T159C)-mCherry (Addgene #35512, obtained from Addgene; the original titer, 3.0×10^{13} copies/ml, diluted to 1/10) or AAV9-Ef1a-mCherry (Addgene # 114470, obtained from Addgene; the original titer, 1.0×10^{13} copies/ml, diluted to 1/10) was injected unilaterally into the left wM1 (AP: 1.0 mm, ML: 1.0 mm, from Bregma, depth: 0.85 mm and 0.35 mm) of wild-type C57BL6/J mice. The injection volume was 200 nl per site. With the scalp sutured, the mice were returned to their home cages for at least three weeks after the AAV injection before behavioral experiments.

Prior to behavioral experiments, mice were implanted with a light-weight metal head-holder.[37] For optogenetic stimulation, pharmacological perturbation, or silicone probe recordings in left wM1, a chamber was made on the left hemisphere by building a wall with dental cement, and a thin layer of glue was applied over the exposed skull. For optogenetic stimulation of deep brain regions,

we used an optical fiber (0.4 mm diameter) attached to a stainless steel ferrule (CFM14L05, Thorlabs) which was implanted over the left NAc (AP: 1.25 mm, ML: 1.5 mm, from Bregma, depth: 3.8 mm) or the left VTA (AP: −3.0 or −3.3 mm, ML: ±0.3 or 0.5 mm, from Bregma, depth: 4.0 mm). The optical fiber cannula was permanently cemented to the skull. For optogenetic stimulation of wM1, we made a small craniotomy over the left wM1 and placed the optical fiber over the craniotomy.

Behavioral tasks

Whisker detection task

To examine the orofacial movements of mice performing a whisker detection task,[10] we analyzed the data obtained from the mice used for recording in our previous paper.[37] The procedure of the whisker detection task was previously described.[37] All whiskers except for the right C2 whisker were trimmed before experiments. We applied a brief (1 ms) magnetic pulse to elicit a vertical deflection of the right C2 whisker transmitted by small metal particles glued on the whisker. The mice under head-fixation were trained to learn the availability of water reward within a 1-s window after the whisker stimulation. The whisker was filmed at 500 Hz with a high-speed camera. The behavioral signals from the lick sensor together with TTL signals to control the water valve and the electromagnetic coil were recorded through an NI board. In some recordings, it was impossible to extract the whisker position due to the metal particles covering the basal part of the whisker. Therefore, we only included the data where the basal part of the whisker was partially exposed. Novice mice had no prior task experience and showed a low hit rate (31.1 ± 4.2%, n = 6 mice). Expert mice analyzed in this study were trained for the task in 8–17 daily sessions before the recording day and exhibited a high hit rate (79.2 ± 3.6%, n = 6 mice).

Auditory Go/No-Go task

At least three days after implantation of the metal head holder, adult male C57Bl6/J mice started to be water-restricted. The mice were adapted to head restraint on the experimental setup through initial training to freely lick the water spout for receiving a water reward (3–5 sessions, one session per day). The mice were then taught, through daily training sessions, to associate a pure tone (2 s) with water availability within a 1-s window after the offset of tone presentation. Trials were started with a 3 kHz tone ("Go" cue) or a 15 kHz tone ("No-Go" cue) following random inter-trial intervals ranging from 3 to 9 s. In some experiments, the "Go" tone and "No-Go" tone were swapped. If the mice licked in the 2 s preceding the time when the trial was supposed to occur, then the trial was aborted, and a subsequent trial started. Lick was detected with a piezo sensor attached to the water spout. After each training session, 1.0–1.5 g of wet food pellet was given to the mouse to keep its body weight above 80% of the initial value. Behavioral control was carried out using a custom-written program on Python interfaced through Arduino Uno. All whiskers except for the right C2 whisker were trimmed before experiments. The whisker was filmed at 200 Hz with a high-speed camera. Behavioral data were acquired using an NI board. Novice mice were defined by poor performance (daily d' < 1.0). These mice were typically on the first day of task training and showed an average hit rate of 33.7 ± 5.5% (n = 9 mice). Expert mice were defined as those keeping a high performance (daily d'> 2.5) for five successive days. These mice showed an average hit rate of 94.1 ± 1.4% (n = 7 mice). One mouse underwent a reversal-learning: after the mouse learned the task with a 3-kHz tone as a Go-cue, then we swapped the Go and No-Go tones. The mouse successfully learned the swapped association, and the data were pooled into the dataset as a different experiment from the initial learning.

Optogenetics

Optogenetic stimulation in head-fixed mice

All the behavioral experiments using optogenetic stimulation followed the habituation of mice to head-fixation for three days. The duration of habituation was ~15 min on the first day, ~30 min on the second day, and ~60 min on the third day. All whiskers were trimmed except the left C2 whiskers or the left and right C2 whiskers before the experiments. For optogenetic stimulation of DA neurons, blue LED (470 nm; M470F3, Thorlabs) light was applied over the VTA or SNc of DAT-ChR2 mice or control Ai32 mice through the implanted optic fiber. For stimulating bReaChES/hrGFP-expressing DA axons in the NAc, green LED (530 nm; M530F2, Thorlabs) light was applied over the NAc through the implanted optic fiber. For stimulating ChR2-expressng neurons in wM1, the blue LED light was applied through the craniotomy made over the left M1. 20 pulses of 5-ms light stimuli were applied at 20 Hz unless otherwise noted. The light power at the fiber tip was 15.8 mW for the blue light and 6.6 mW for the green light unless otherwise noted. The frontal mouse face, including its nose and whisker(s), was filmed at 500 Hz from above with a high-speed camera. Through immunostaining (see below), we routinely checked the location of implanted optical fiber and discarded data when the fiber tip was found to be more than 0.5 mm away from the target or inserted too deep damaging the target brain structure.

Sound-oDAS pairing conditioning

For the Pavlovian sound-oDAS conditioning, we used the mice that experienced oDAS. We habituated the mice to a 15-kHz tone presentation (5 s) by being exposed to the tone stimuli 20 times with random intervals of 60–120 s under head fixation on the day before starting the conditioning. For the conditioning, we presented to the mice the 15-kHz sound cue (5 s) paired with oDAS (5 ms, 20 times at 20 Hz) at the last 1 s of the cue. The inter-trial interval was set randomly for each trial to be from 180–240 s. A custom-written program on Python interfaced through Arduino Uno controlled the timings of sound cue presentation and light stimulation, which were synchronized with filming the mouse's frontal face from above. The mice experienced ~20 paired stimuli in each daily session.

Pharmacological perturbation

To examine the effect of a D1R antagonist on orofacial movements, we first calculated the injection volume of SCH23390 (0.3 mg/kg) or raclopride (3 mg/kg) for each experimental mouse and injected saline of the calculated volume intraperitoneally into the mouse. The behavioral recording was started 15 min after injection. After the recording session with saline injection, the mice were subjected to an IP injection of the D1R/D2R antagonists, and the behavioral recording was resumed 15 min after injection.

To examine the effect of wM1 inactivation on orofacial experiments, we first made a small craniotomy over wM1 of DAT-ChR2 mice under anesthesia. After recovery from anesthesia, the mouse was head-fixed to the experimental setup, and the behavior was recorded. Subsequently, 100 nl of Ringer's solution with or without muscimol (5 mM) was injected into at 900, 700, 500, 300, and 100 μm each below the surface using a glass pipette inserted through the craniotomy. A small volume of Chicago Sky Blue was mixed in the muscimol solution. The whole injection period was 20–30 min. The behavioral tests were resumed after the injection pipette was slowly withdrawn.

Immunostaining

After behavioral and electrophysiological experiments, we routinely performed transcardial perfusion of the mice with 4% paraformaldehyde (PFA). The brain was removed and incubated with 4% PFA solution overnight for post-fixation. The fixed brain was then kept in phosphate buffer (PB) until further processing. The fixed brain was sectioned into coronal slices on a vibratome (section thickness: 100 μm). For immunostaining of brain slices, the slices were washed three times with a blocking buffer containing 1% bovine serum albumin and 0.25% Triton-X in phosphate buffer saline (PBS) and then incubated with primary antibodies (anti-tyrosine hydroxylase, rabbit polyclonal, 1:1000, Merck Millipore; anti-D1R, guinea pig polyclonal, 1:200, Frontier Institute; anti-GFP, mouse monoclonal, 1:1000, Fujifilm Wako Chemicals) in the blocking buffer overnight at 4 °C. The slices were then washed three times with the blocking buffer and then incubated with secondary antibodies (CF594-conjugated donkey anti-rabbit IgG, 1:1000, Biotium; CF488A-conjugated goat anti-mouse IgG, 1:1000, Biotium; CF594-conjugated donkey anti-guinea pig IgG, 1:1000, Biotium) in the blocking buffer for 1–2 h at room temperature (RT). Cellular nuclei were stained by incubation for 10–15 min with DAPI (2 μM in PB) at RT. The stained samples were mounted using DABCO and observed under a fluorescence microscope (BZ-9000, Keyence). Images were saved using BZ-X Viewer (Keyence).

Electrophysiology

A small craniotomy was made over the left wM1 (1 mm anterior, 1 mm lateral from Bregma). Extracellular spikes were recorded in head-fixed mice using a silicon probe (A1x32-Poly2-10mm50s-177, NeuroNexus) with 32 recording sites along a single shank, covering 775 mm of the cortical depth. The probe was lowered gradually until the tip was positioned at a depth of 1.0–1.1 mm under the wM1 pial surface. The craniotomy site was then covered with 1.5% agarose dissolved in Ringer's solution. Neural data were filtered between 0.5 Hz and 7.5 kHz, amplified using a digital head-stage (RHD2132, Intan Technologies), and digitized with a sampling frequency of 30 kHz. The digitized neural signal was transferred to an acquisition board (Open Ephys) and stored on an internal HDD of the host PC for offline analysis. The TTL pulses for the sound and light stimulation were also recorded through the Open Ephys acquisition board. Spiking activity on each probe was detected and sorted into different clusters using Kilosort (https://github.com/cortex-lab/KiloSort). After an automated clustering step, clusters were manually sorted and refined using Phy (https://github.com/cortex-lab/phy). Only well-isolated single units (174 units) were included in the dataset.

QUANTIFICATION AND STATISTICAL ANALYSIS

Motion energy analysis

Mouse facial movements were quantified by analyzing the side-view (Figure 2B) and top-view (Figure 2C) movies. Motion energy was computed as the absolute value of the difference of consecutive frames obtained during oDAS (for 1 s) and at the baseline (0–1 s before the stimulus onset). The motion energy heat-map is shown as the difference between motion energy during oDAS and at the baseline in each pixel. For quantification (Figure 2B), we set polygonal regions of interest around the ear or orofacial area and calculated the mean change in motion energy evoked by the oDAS by comparing values during oDAS and at baseline.

Analysis of whisker movements

Movements of the right C2 whisker were quantified offline with ImageJ using an open source macro (https://github.com/tarokiritani/WhiskerTracking) and the data were analyzed with Igor Pro or MATLAB. The total whisker movements (ΣWM) were calculated as the cumulative WMs during oDAS (Figures 2, 4, 5, S2, S3D, and S6), at 0–1 s after the reward time window for the data in the reward-based learning tasks (Figure 1) or at 0–0.5 s after the cue onset in the sound-oDAS pairing task (Figures 4H, 4J, S3B, S4G, S4I, S5B, and S6A). Data with the prominent whisking starting during the 1-s period before the onset of oDAS (Figures 2, 4, 5A–5D, 7, S2, S4, S5A, and S5C) or the conditioning stimulus (Figures 3, 4G-4I, 5E–5H, 6, S3, S4F-S4I, S5B, S6, and S7) were excluded from the analysis. When the ΣWM during oDAS exceeded 90 deg, the data were defined as epochs with whisking induced (WM+). A cue-locked WP was defined as a WP of more than 5 deg above baseline within 0.5 s after the onset of cue presentation. The onset time of WM or WP was taken as the time at which the whisker angle exceeded 1 deg above baseline, among these epochs with WM or cue-locked WP.

Analysis of nose movements

We quantified nose movement using the markerless video tracking software, DeepLabCut.[38] As illustrated in Figure 2G, we manually annotated the five points of the top-view nose (left and right anterior/posterior edges and nose tip) using 60–340 frames per movie to train a deep neural network. An estimated position with a low likelihood (<0.8) was omitted and replaced with a pixel value obtained using linear interpolation of neighboring values.[55] The nose area was the area of the pentagon formed by the estimated five points. The nose length in the anterior-posterior axis was taken as the distance between the nose tip and the middle point of the posterior nose edges. The lateral movement of the nose tip was the displacement of the horizontal coordinate of the nose tip quantified as the percentage with the average anterior-posterior nose length taken as 100%. The onset of lateral nose tip movement was defined as the time point where the trace exceeded three times of standard deviation of the baseline (0–1 s before the stimulus/cue onset). The latency of nose movement was defined as the time difference between the stimulus/cue onset and the onset of lateral nose tip movement. The data with whisking at the pre-stimulus period (1 s) were excluded from the analysis of nose movement.

Machine learning models

We utilized machine learning models to decode trial categories ("Hit" or "CR") of the auditory Go/No-Go task using whisker time plots. We selected "Hit" and "CR" trials from the dataset while excluding "Miss" and "False Alarm (FA)" trials. We filtered the data for each trial with a band-pass filter (4–20 Hz) and transformed it into a power spectrogram using short-term Fourier transformation with 200-ms or 100-ms bins. The power spectrogram was then extracted at 4-20 Hz and linearly normalized so that the sum of powers equaled one in each time bin. We created power spectrum matrices with 240 dimensions (24 frequency domains x 10 time domains) for the data during the cue period (2 s) or 0-1 s after the reward time window (after RA). Among the data from seven expert mice, we pooled the data from six mice as training data, excluding the one from one mouse as test data, and applied the principal component analysis (PCA) on MATLAB to make a PC space with two dimensions. We used this PC space to obtain the first and second PC scores for each trial of the test data and plotted them (Figure S1C). We constructed a logistic regression model using the PC plot obtained from training data, which outputs a likelihood (minimum: 0, maximum: 1) of being "Hit" for each trial of the test data. The trials with a likelihood of more than 0.5 were predicted as "Hit" trials, and otherwise, the trials were predicted as "CR" trials. The decoding accuracy is a fraction of the number of correct predictions over the total trial number of the test data. We repeated the same procedure for the other six mice (a process called leave-one-subject-out cross-validation).

We also used leave-one-subject-out cross-validation to train logistic regression models for discriminating between cue-locked and reward-aligned WMs during the auditory Go/No-Go task (Figure 1H), oDAS-aligned and cue-locked orofacial movements during the sound-oDAS pairing task (Figures 3H and 3I), WMs during the sound-oDAS pairing task and those during the auditory Go/No-Go task (Figure 3J), WMs with different wM1 stimulus patterns (Figure 7F), and wM1-driven WMs and those in the sound-oDAS pairing task (Figure 7G). As decoding features, we used the amplitude, total movements, and first PC score of multidimensional power spectrum matrices (see above) of whisker (W-amp, ΣWM, and W-spectral PC) and/or nose (N-amp, ΣNM, and N-spectral PC) obtained from 1-second traces during the cue onset, after RA, during oDAS or upon wM1 stimulation.

Classification of single units

Single units recorded with the silicone probe were classified as fast-spiking (FS) putative interneurons or regular-spiking (RS) putative pyramidal cells based on their trough-to-peak time of average spike waveform. Single units with a trough-to-peak time < 0.35 ms were classified as FS cells, and units with a trough-to-peak time > 0.35 ms were classified as RS cells.

Analysis of the correlation between spike rates and whisker behavior

We classified wM1 cells based on their correlation with whisker behavior during the sound-oDAS pairing tests. We first categorized the trials into four categories (Figure 6A): "CL+OA trials" are trials with both cue-locked WP and oDAS-aligned WM; "CL trials" are trials with cue-locked WP but without oDAS-aligned WM; "OA trials" are trials with oDAS-aligned WMs but without cue-locked WP; and "No reward-related WMs trials" are trials with neither cue-lockedWP nor oDAS-aligned WM. We used different trial categories: "Cue-WP+ trials" are CL+OA and CL trials; "Cue-WP- trials" are OA and No reward-related WMs trials; "oDAS-WM+ trials" are CL+OA and OA trials; and "oDAS-WM- trials" are CL and No reward-related WMs trials. We defined the cellular categories as follows: "CL+OA cells" showed a significantly higher firing rate at the cue onset (1 s) in Cue-WP+ trials than in Cue-WP- trials, and also showed a significantly higher firing rate during oDAS in oDAS-WM+ trials than in oDAS-WM- trials; "CL cells" showed a significantly higher firing rate at the cue onset (1 s) in Cue-WP+ trials than in Cue-WP- trials, and exhibit similar firing during oDAS in oDAS-WM+ and oDAS-WM- trials; "OA cells" showed a significantly higher firing rate during oDAS in oDAS-WM+ trials than in oDAS-WM- trials, and exhibit similar firing at the cue onset (1 s) in Cue-WP+ and Cue-WP- trials. In Figure 6E, we plotted "CL correlation" as the Pearson correlation coefficients between spike rates and the maximal WP amplitudes during 1 s at the cue onset and "OA correlation" as the Pearson correlation coefficients between spike rates and the variances of the whisker position during oDAS. For motion-triggered PSTHs upon oDAS (Figure 6I), the data with whisking at 0–0.2 s before oDAS were excluded from the analysis.

Statistics

All values are expressed as mean ± SEM except for the boxplots in the figures. Boxplots indicate median and 1st/3rd quartile, with whiskers showing maximal and minimal data points. Statistical tests were performed using GraphPad Prism. The normality of data distribution was routinely tested. Analyses of two sample comparisons were performed using unpaired or paired *t* tests when each

sample was normally distributed, or Wilcoxon signed rank test (paired) or Mann-Whitney *U* test (unpaired) when at least one of the samples in every two-sample comparison was not normally distributed. Tests for two-sample comparison were two-sided. Statistical analyses for multiple comparisons were carried out using one- or two-way ANOVA followed by Bonferroni's multiple comparison tests or Dunnett's multiple comparison tests vs. the control, unless otherwise noted. For correlation analysis, Pearson's correlation coefficient (*r*) for normally distributed sets of data or Spearman's rank correlation coefficient (rho) for randomly distributed data was calculated.